AGU PUBLICATIONS

Journal of Advances in Modeling Earth Systems

RESEARCH ARTICLE

10.1002/2016MS000861

Modeling the air-sea feedback system of Madeira Island

Julie Pullen[1], Rui Caldeira[2,3], James D. Doyle[4], Paul May[5], and Ricardo Tomé[6]

[1]Department of Civil, Environmental and Ocean Engineering, Stevens Institute of Technology, Hoboken, New Jersey, [2]Oceanic Observatory of Madeira, Agência Regional para o Desenvolvimento da Investigação Tecnologia e Inovação, Funchal, Portugal, [3]CIIMAR & CIIMAR-Madeira—Interdisciplinary Centre of Marine and Environmental Research, Porto & Madeira Island, Portugal, [4]Marine Meteorology Division, Naval Research Laboratory, Monterey, California, [5]CSRA, Monterey, California, [6]Instituto Dom Luiz, Faculdade de Ciências, Universidade de Lisboa, Lisbon, Portugal

Key Points:
- Atmospheric wakes and vortex shedding promote cloud-free island lee region
- Oceanic warming and interaction with atmospheric boundary layer occur in island wake in a coupled air/sea model
- Nocturnal drainage winds aid ocean diurnal warm layer dissipation

Correspondence to:
J. Pullen,
Julie.Pullen@stevens.edu

Citation:
Pullen, J., R. Caldeira, J. D. Doyle, P. May, and R. Tomé (2017), Modeling the air-sea feedback system of Madeira Island, *J. Adv. Model. Earth Syst.*, *9*, 1641–1664, doi:10.1002/2016MS000861.

Received 9 NOV 2016
Accepted 12 JUN 2017
Accepted article online 19 JUN 2017
Published online 10 JUL 2017

Abstract A realistic nested data-assimilating two-way coupled ocean/atmosphere modeling study (highest resolution 2 km) of Madeira Island was conducted for June 2011, when conditions were favorable for atmospheric vortex shedding. The simulation's island lee region exhibited relatively cloud-free conditions, promoting warmer ocean temperatures (∼2°C higher than adjacent waters). The model reasonably reproduced measured fields at 14 meteorological stations, and matched the dimensions and magnitude of the warm sea surface temperature (SST) wake imaged by satellite. The warm SSTs in the wake are shown to imprint onto the atmospheric boundary layer (ABL) over several diurnal cycles by modulating the ABL depth up to ∼200–500 m. The erosion and dissipation of the warm ocean wake overnight was aided by atmospheric drainage flow and offshore advection of cold air ($\Delta T = 2°C$) that produced strong upward heat fluxes (∼50 W/m^2 sensible and ∼250 W/m^2 latent) on an episodic basis. Nevertheless, the warm wake was never entirely eroded at night due to the cumulative effect of the diurnal cycle. The spatial pattern of the diurnal warming varied day-to-day in location and extent. Significant mutual interaction of the oceanic and atmospheric boundary layers was diagnosed via fluxes and temperature cross sections and reinforced by sensitivity runs. The simulation produces for the first time the interactive nature of the ocean and atmosphere boundary layers in the warm wake region of an island with complex terrain.

1. Introduction

Accurate forecasting of coastal oceanic and atmospheric circulation is particularly challenging in island regions due to a number of factors [*Caldeira et al.*, 2016]. From a geographical perspective, many islands possess steep terrain and heterogeneous microclimates. The resulting atmospheric circulation depends crucially on the scale of the mountains, with high terrain (and suitable Froude number) producing complex features such as mountain wave breaking and vortex shedding [*Schär and Smith*, 1993a,b]. Microclimates on islands can encompass desert, alpine, rainforest and urban regions, with associated soil moisture and hydrologic characteristics that alter the surface roughness and the lower boundary layer [*Teixeira et al.*, 2014]. Ocean features generated by islands (such as mesoscale eddies, filaments and warm wakes) generate distinct sea surface temperature signatures [e.g., *Sangrà et al.*, 2007]. These patterns in turn feedback to the overlying atmosphere [*Xie et al.*, 2001] and render an island-modulated circulation that is fundamentally a two-way coupled environment. Thus, islands represent an important geographical setting for realistic earth system models to emulate.

Thermal effects lead to several types of atmospheric flow regimes on islands. Sea-land breeze systems become established on spatially large islands. And differential local slope heating can modulate the larger-scale circulation system. In addition, nocturnal drainage flows deliver cool, dry mountain air down into valleys and often out to sea under the influence of gravity [*Petkovšek and Hočevar*, 1971]. Such flows are commonly termed katabatic.

Island drainage winds generally enhance the land breeze, but the former occurs in a much shallow layer near the surface (10–100 m depth) [*Cuxart et al.*, 2007]. Also, the magnitude of episodic drainage flows can be stronger than diurnal offshore land breezes (3–10 m/s compared with <3 m/s), especially in steep complex terrain. The spatial influence of the land breeze over the sea can vary (25–100 km) [*Gille et al.*, 2005;

Lefèvre et al., 2010] while that of the katabatic flow is estimated to be ~25 km [*Alpers et al*., 1998; *Li et al*., 2007; *Galvin*, 2015]. Finally, the katabatic flow can oppose the larger-scale winds (e.g., trades or synoptic conditions) when it occurs on the windward side of the island [*Feng and Chen*, 2001; *Cécé et al*., 2014]. Many well-studied islands are situated in trade wind regimes, and prior work has focused on examining weak, medium, and strong winds and their interactions with thermal circulations [*Melas et al*., 2000; *Lefèvre et al*., 2010].

The conditions for atmospheric wake formation and vortex shedding in the lee of islands have been explored from theoretical, computational, and observational perspectives in diverse geographical settings (e.g., *Smith and Grubišic* [1993] for Hawaii; *Smith et al*. [1997] for St. Vincent). On steep islands with upwind flow conditions creating Froude number <0.4, Von Kármán vortex streets commonly occur [*Etling*, 1989].

Early remote sensing studies revealed intense vortex shedding downwind of Madeira [*Chopra and Hubert*, 1965]. Subsequent recent atmospheric wake numerical studies and targeted sampling refined the understanding of the complex wake region of Madeira [*Nunalee and Basu*, 2014; *Grubišić et al*., 2015]. Vortex shedding events are most frequent in June–August when the ABL depth is below mountain-top (<1500) and capped by a strong inversion, thereby favoring resonant interactions with the terrain [*Grubišić et al*., 2015].

Warm sea surface temperatures are frequently found in the lee of islands [*Caldeira et al*., 2002]. *Caldeira and Tomé* [2013] hypothesized that the cloud-free conditions of atmospheric wakes promote enhanced short wave radiation and lee-side ocean warming. *Caldeira and Marchesiello* [2002] measured the upper ocean warming (<20 m depth) downwind of the Catalina Islands to be 4–5°C above the surrounding oceanic waters. *Caldeira et al*. [2002] and R. Caldeira (personal communication, 2012) measured this effect in situ, leeward of Madeira to be 2–3°C concentrated in the upper 10–20 m. The Madeira warm wake extends over 100 km offshore during summertime. Similar characteristics of warm wakes have been discovered in the lee of the Canary Islands [*Barton et al*., 2000]. And wake regions can have long-ranging effects (>300 km), as discovered in Hawaii [*Smith and Grubišic*, 1993; *Hafner and Xie*, 2003].

Reduced lee-side winds due to terrain blocking are expected to suppress ocean mixing, further contributing to the near-surface oceanic warming. Indeed, there is a sharp contrast between the calm winds in the lee and the strong winds at the island flank that manifests in the sea state and SST [*Grubišić et al*., 2015]. The correlation between high SST and low winds was robust during the Madeira measurement campaign, Island-induced Wake (I-WAKE).

Though lacking a coupled air/sea model, *Grubišić et al*. [2015] were able to demonstrate improved atmospheric model skill through uniformly increasing the SST by 2.5°C. Specifically, this adjustment enhanced the ABL turbulence and increased the ABL temperatures to better match the dropsoundes. The result was an elevation of the ABL by ~200 m in the model. Furthermore, *Caldeira and Tomé* [2013] suggest that atmospheric wake characteristics (e.g., strong/vortex shedding regime versus weak/no-shedding regime) can be influenced by SST feedback. These studies, along with *Caldeira et al*. [2016], point to the importance of interactive two-way coupled modeling for accurately simulating island wake regions.

Coupled model simulations have been conducted for several archipelagos. *Pullen et al*. [2008, 2011] utilized the Coupled Ocean-Atmosphere Mesoscale Prediction System (COAMPS®) at high resolution to probe wind/ocean eddy interactions in the Philippines. Those simulations revealed the importance of resolution in capturing the detailed curl pattern generated by atmospheric flow around mountainous island terrain. In that tropical setting the strong wind stress curl from atmospheric cold surges induced double gyre oceanic eddy formation. In subsequent work, the model was used to document rainfall extremes in the Philippines derived from the interaction of orography with multiple factors operating across several time scales [*Pullen et al*., 2015]. In another island application of COAMPS, *Chen et al*. [2010] contrasted atmospheric wakes generated by coupled and uncoupled simulations of California's Channel Islands.

Here the realistic coupled model COAMPS is used to examine air-sea interaction in the warm wake region of the island of Madeira. To our knowledge, this is the first implementation of a high-resolution coupled ocean-atmosphere modeling system focused on island warm wake air-sea feedback. Supported by observations (including satellite and meteorological station measurements) we document the evolution of the oceanic and atmospheric boundary layers during several days in the summertime, when lee vortex shedding in the atmosphere is most pronounced.

This study probes how warm wake waters surrounding the island impact the atmosphere, and investigates how episodic nocturnal winds modify air/sea fluxes and imprint on the boundary layer diurnal evolution. Although warm wake formation is robust throughout the summertime in Madeira, we focus on 14–15 June 2011 when atmospheric vortex shedding and a warm wake coincide with strong drainage winds along the coast and over the sea. We contrast this with a case of atmospheric vortex shedding with no drainage winds on 18–19 June 2011. We also examine a set of sensitivity runs designed to isolate the role of two-way coupling.

The model description and implementation details (section 2.1) are followed by an overview of Madeira Island geography (section 2.2) and observations (section 2.3). The results are presented in section 3. Section 3.1 describes the atmospheric wake regimes, while section 3.2 details the formation of the oceanic warm wake over a diurnal cycle. The interaction of the warm wake with a nocturnal drainage flow is presented in section 3.3. Section 3.4 addresses how the ocean and atmosphere boundary layers evolve over several days, including during the sensitivity runs. We conclude with a summary and discussion (section 4).

2. Methods

2.1. Coupled Modeling System

The two-way coupled model configuration is described first, followed by a description of the individual model constituents. The atmospheric model domains are of 18, 6, and 2 km resolution (Figure 1). The ocean model is configured on one domain at 2 km resolution under the third (innermost) atmosphere model domain.

The atmosphere and ocean models exchange flux information at a time interval of 6 min using the Earth System Modeling Framework (ESMF). Heat, moisture, and momentum exchange coefficients are based on

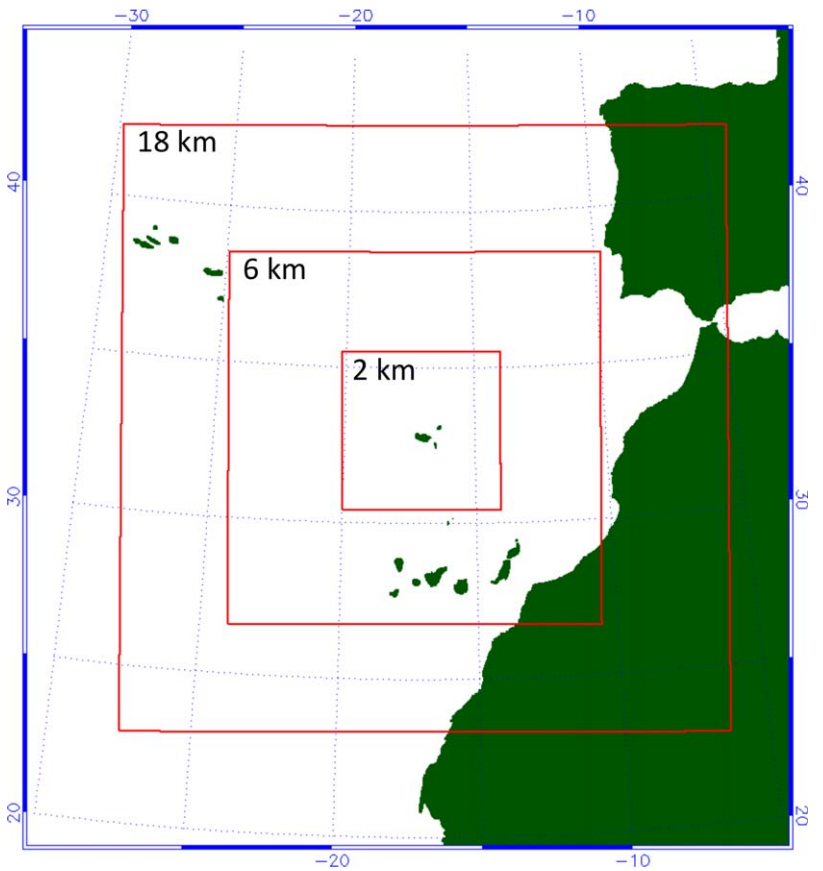

Figure 1. The domains of the COAMPS simulation. The atmosphere model is run for the 18, 6, and 2 km nested domains. The ocean model is run in two-way interactive mode with the atmosphere for the innermost nest (2 km resolution).

the COARE3.0 bulk flux algorithms of *Fairall et al*. [2003], as detailed in *Chen et al*. [2010]. *Allard et al*. [2010] gives a comprehensive description of the coupled model components and architecture. Specific settings in the model are described below.

The ocean and atmosphere have 50 and 60 vertical levels, respectively. Highest vertical resolution is concentrated near the surface. In fact, the ocean model has 16 levels in the upper 50 m, and 33 in the upper 500 m. Coupled model initiation and boundary conditions are derived from the Navy's global models: Navy Operational Global Atmospheric Prediction System (NOGAPS, atmosphere) and Navy Coastal Ocean Model (NCOM, ocean). Outside the 2 km ocean domain, SSTs are prescribed from global NCOM.

The model simulations are carried out for 1–20 June 2011. Eighteen hour forecasts are conducted every 12 h. Hourly or three-hourly model fields are utilized in the analysis.

2.1.1. Ocean

The ocean model, NCOM, is a three-dimensional, primitive-equation, free-surface model using the hydrostatic, Boussinesq, and incompressible approximations as detailed in *Martin* [2000] and *Barron et al*. [2006]. NCOM uses a hybrid sigma and z-level vertical grid with sigma coordinates applied from the surface down to a specified depth, with level coordinates used below that. The model equations are solved on a staggered, Arakawa C-grid. Temporal differencing is a leap-frog formulation with an Asselin filter to suppress time splitting. Spatial averages and finite differences are mainly second order with an option for higher-order formulations for advection. The propagation of surface waves and vertical diffusion is treated implicitly. The model uses the Mellor-Yamada Level 2.5 turbulence scheme [*Mellor and Yamada*, 1982] for vertical mixing. The 3-D variational ocean data assimilation system Navy Coupled Ocean Data Assimilation (NCODA) system [*Cummings*, 2005] is activated for the first 7 days (1–7 June) of the simulation in order to create a more realistic representation of the ocean state. Tides are not used in this simulation.

2.1.2. Atmosphere

The atmospheric model is nonhydrostatic and possesses a terrain-following vertical coordinate as described in *Hodur* [1997]. The compressible equations are integrated using a time splitting technique with a semi-implicit formulation for the vertical acoustic modes. A prognostic equation for the turbulence kinetic energy (TKE) budget is used to represent the planetary boundary layer and free-atmospheric turbulent mixing and diffusion [*Hodur*, 1997]. The *Louis* [1979] surface-layer parameterization, which makes use of a surface energy budget based on the force-restore method, is used to represent the land surface fluxes. Subgrid-scale moist convection is represented using the *Kain and Fritsch* [1993] parameterization. The grid-scale evolution of the moist processes is predicted explicitly from budget equations for cloud water, cloud ice, raindrops, snowflakes, and water vapor modified from *Rutledge and Hobbs* [1983]. Resolutions below 10 km do not utilize convective parameterization and the cloud microphysics is used on all grid meshes. An advanced radiation parameterization following *Fu and Liou* [1992] is used to allow for aerosol, cloud, and radiation-interactions. The 3-D NRL Atmospheric Variational Data Assimilation System (NAVDAS) [*Daley and Barker*, 2001] is utilized for the simulation at a 12 h update cycle.

Results from COAMPS model simulations have been evaluated on numerous occasions using special observations and field campaign datasets and have been demonstrated to accurately simulate mesoscale flows influenced by topography [e.g., *Doyle et al*., 2011, 2009; *Jiang and Doyle*, 2009; *Reinecke and Durran*, 2009].

2.2. Geographical Setting

The archipelago of Madeira is situated in the subtropics. It consists of three islands, with the largest being Madeira (22 km $\times$ 57 km). The volcanic mountains are positioned in a northwest-southeast oriented spine of high terrain through the central portion of the island (Figure 2). The main peaks attain 1818 m (Pico Arieiro), 1852 m (Pico das Torres), and 1861 m (Pico Ruivo) heights in a cluster at approximately $-16.93°$W. Extending laterally from the peaks are highlands ($>$1000 m) deeply chiseled by river ravines draining to the coasts. The highlands are more pronounced to the west. To the east the land is dry, windswept and desert like. The climate shifts from subtropical rainforest to alpine along the mountain slopes. The main city of Funchal lies on the southeast coast. Porto Santo, a smaller island northeast of the main island of Madeira, possesses low terrain (under 500 m). The local time in summer is UTC (Z) $+1$.

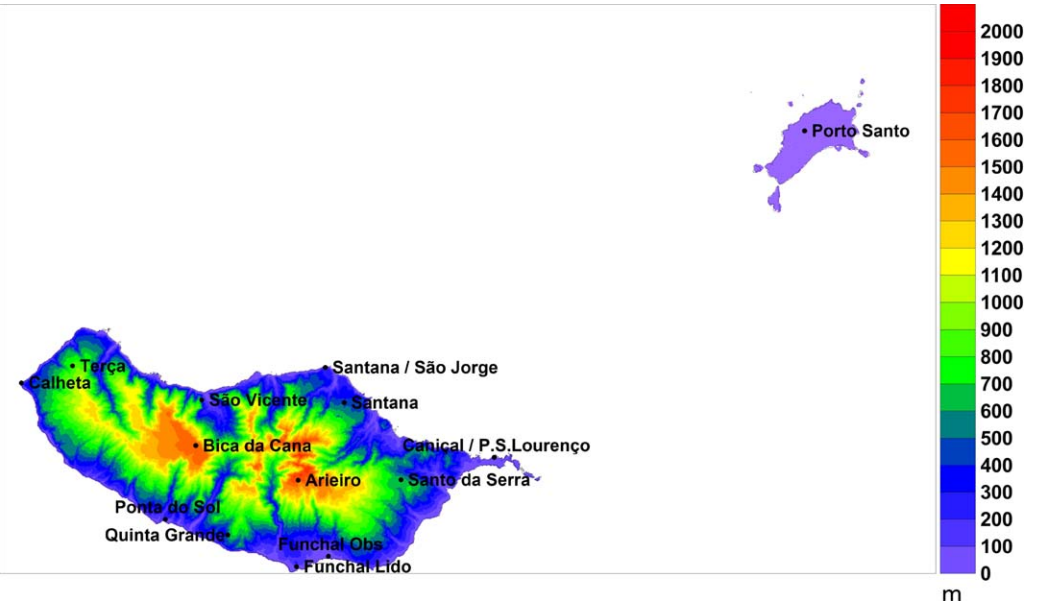

Figure 2. Map and terrain of the Madeira archipelago. The locations of meteorological stations are indicated.

Offshore the bathymetry is shallow to the southeast of Madeira Island. An ocean ridge of ∼100m depth connects Madeira Island with the flat Desertas Island off the southeast flank (Figure 1). Elsewhere a steep shelf plunges ∼4000 m within 50 km offshore of the south coast of Madeira.

2.3. Observations

The satellite measurements used here were retrieved from the Moderate Resolution Imaging Spectroradiometer (MODIS) imagers on the Terra and Aqua Earth Observing System (EOS) platform. The instruments capture data from 36 spectral bands and varying spatial resolutions and are capable of viewing the earth's surface every 1–2 days. The MODIS Aqua L3 SST average at 4 km resolution consists of sea surface temperature derived from the satellite thermal IR bands, and visible imagery from multiple bands.

In this study we also use station observations provided by the Portuguese Meteorological Institute (IPMA, Instituto Português do Mar e da Atmosfera). A total of 13 meteorological stations spread across Madeira Island and one on Porto Santo Island were used (Figure 2). Observations at 2 m height consist of hourly measurements of air temperature, relative humidity, sea level pressure, and surface pressure. Some stations also report measurements of wind, precipitation, and radiation. Modeled fields are extracted at the closest grid point to the station latitude and longitude, and checked to ensure they are on land in the model.

3. Results

3.1. Atmospheric Conditions

Steady northeasterly trade winds from the Azores high-pressure system dominate the summer months—with winds ∼5 m/s below the inversion, rising to ∼10 m/s above the inversion [*Grubišić et al.*, 2015]. The position of the Azores high during the summer months aligns the winds generally perpendicular to the mountains, favoring terrain-induced perturbations such as gravity waves, lee vortices, and tip jets [e.g., *Doyle and Shapiro*, 1999].

In June 2011, winds from the station and model are 5–8 m/s at upwind and mountain-top sites (Figure 3). The seasonal NE trade winds are dominant at this time, but there is more directional variability at Porto Santo relative to Arieiro in both the model and measurements. Overall COAMPS winds are somewhat weaker relative to the observations.

Boundary layer heights decrease through the summer season to a minimum in August of 750–1250 m (thus below mountain-top), with a corresponding increase of wake events that peaks in August [*Grubišić et al.*, 2015]. On 14 June 2011 the modeled ABL height at upwind location Porto Santo Island was ∼750 m,

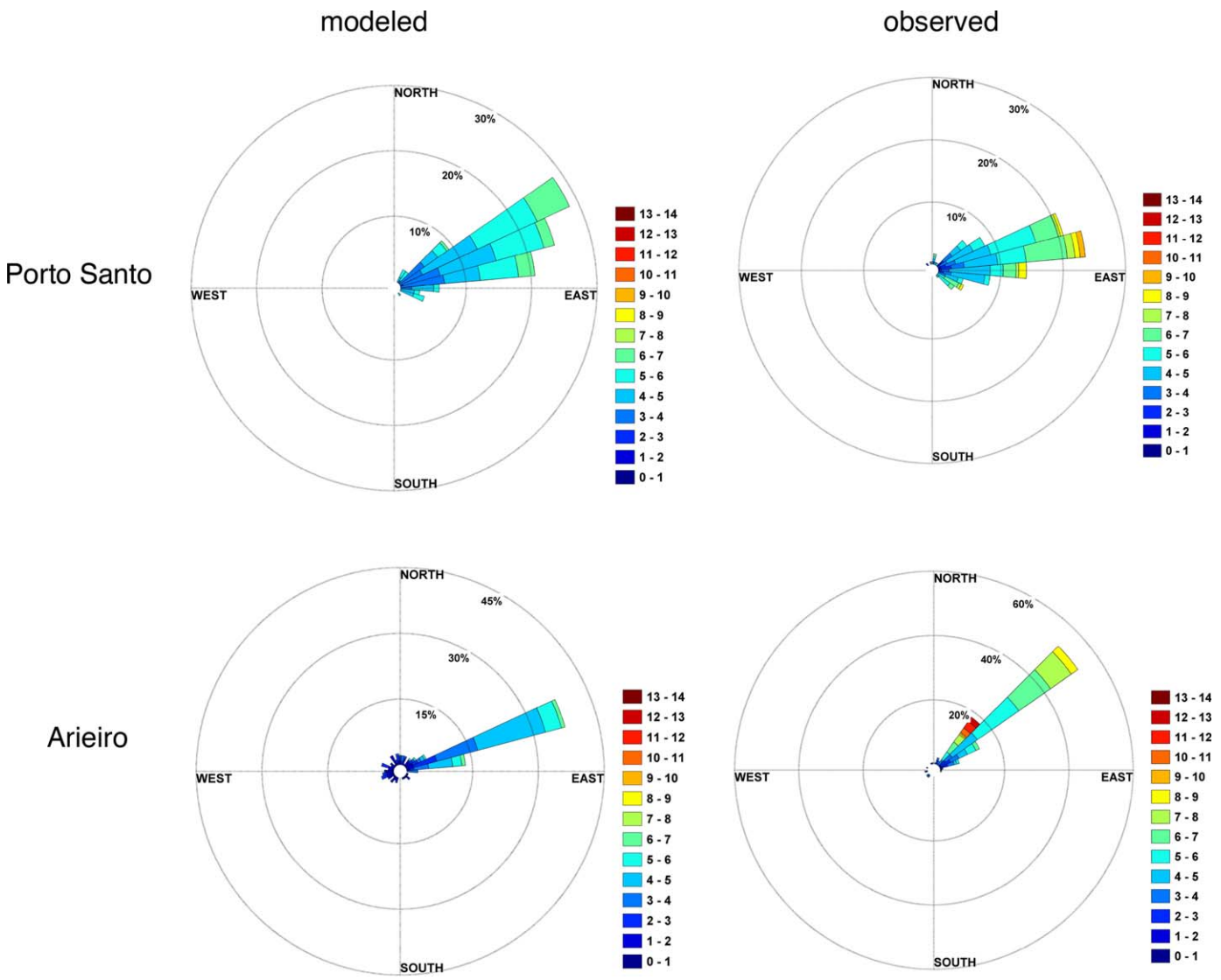

Figure 3. (top) Upwind Porto Santo island and (bottom) mountain-top Arieiro station winds (m/s) for (left) COAMPS and (right) observations during 10–20 June 2011. Station locations are shown in Figure 2.

decreasing to <500 m on 15 June (not shown). At Porto Santo, air temperature and sea level pressure model-data correlation is high (Figure 4). The model possesses a somewhat stronger diurnal cycle, particularly at night.

Modeled air temperature is compared with measured values at the 14 stations (Table 1). Correlations are above 0.7 and biases are generally under 2°C. Variations in modeled-observed agreement are tied to the station location. The overall greatest discrepancies are found at mountain-top (Arieiro) and at northwest site Terça. Funchal Observatory also exhibits weaker agreement for RMSE and mean absolute error (MAE). The overall best agreement is attained at island site Porto Santo (upwind of Madeira), Santana and São Vicente (on northern central coast of Madeira). Of the southern coast station locations, Quinta Grande exhibits the closest correspondence.

As in *Lefèvre et al*. [2010], orography exerts a strong control on the fine-scale model-data wind comparison. Accordingly, the best wind skill assessment was obtained in the "mountain-less" island of Porto Santo ($R = 0.64$), as well as in upwind stations directly exposed to the oncoming (synoptic) winds, such as Santana/São Jorge ($R = 0.64$), Santo da Serra ($R = 0.65$), and Caniçal/P.S. Lourenço ($R = 0.64$). As with air temperature, greatest errors are found at Arieiro and Terça. Station data are necessarily compared with

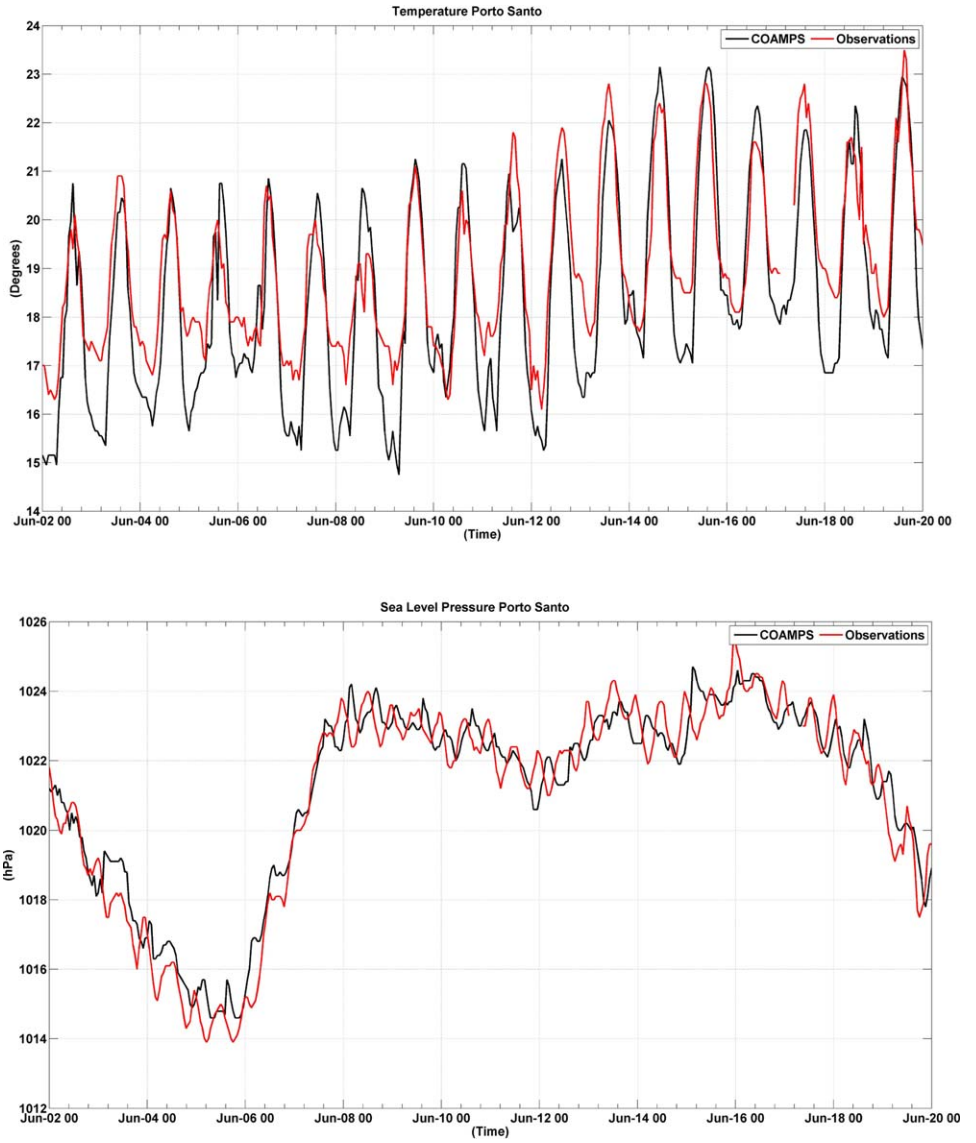

Figure 4. Upstream conditions consisting of near-surface air temperature and sea level pressure measured (red) and modeled (black) on the Island of Porto Santo. The station location northeast of Madeira Island is shown in Figure 2.

model fields extracted from approximate locations on the model grid, which further exacerbates discrepancies.

Atmospheric vortex shedding in the lee of Madeira is evident on 14 June 2011 (Figure 5). Marine stratocumulus cloud distributions permit the visualization of the size and extent of lee vortices. The vortices persist for over 500 km downwind. Modeled fields of total cloud cover and wind stress curl denote relatively cloud-free areas (Figure 5) and potential vorticity banners (not shown) associated with the lee vortex shedding. The effects are visible several hundred kilometers downwind. On the following day (15 June) the vortex shedding has subsided and more lee clearing is found in the model. Hence the dynamic lee region represented in the coupled model is in general agreement with the satellite cloud image from the same day, and revealed a weak wake (no vortex shedding) with more lee clearing on the subsequent day.

Wind stress curl maps of the shear zones are good proxies for vortex activity (Figure 6). Besides revealing details of the strong-to-weak wake transition on 14–15 June, it shows a weak-to-strong wake transition on 18–19 June where no vortex shedding is replaced by atmospheric lee vortex shedding on the subsequent day.

Table 1. Model-Observed Near-Surface Temperature Comparison for 10–20 June 2011[a]

Temperature (°C)	R	RMSE	BIAS	MAE
Funchal Obs	0.89	3.12	−1.70	2.64
Porto Santo	0.91	0.76	−0.03	0.62
Santana/São Jorge	0.81	1.55	−0.45	1.28
Santana	0.89	1.47	1.02	1.19
São Vicente	0.91	2.00	−1.63	1.74
Bica da Cana	0.90	3.07	−2.46	2.61
Funchal Lido	0.83	2.54	−1.25	2.14
Arieiro	0.75	3.75	0.94	3.18
Santo da Serra	0.85	2.32	−0.49	1.56
Caniçal/P. S. Lourenço	0.77	1.42	0.51	1.07
Terça	0.69	3.08	0.86	2.58
Quinta Grande	0.90	2.18	−1.36	1.76
Ponta do Sol	0.89	2.92	−2.58	2.62
Calheta	0.92	2.09	1.25	1.63

[a]Station locations are shown in Figure 2. R is correlation, RMSE is root-mean-square error, and MAE is mean absolute error.

For inversions located below mountaintop the orography represents a significant (blocking) obstacle and flow splitting is prone to develop upstream, leading to tip jets on the flanks of the island [*Petersen et al*., 2005]. Tip jets are evident in the strong shear regions on the west and east sides of Madeira (Figures 6 and 11). Other localized features such as a wind stress curl couplet generated by Porto Santo Island, and cloud-free regions in the lee of the Canary Islands are also apparent in the simulation.

3.2. Oceanic Warm Wake Evolution

The downwind region of Madeira exhibits warming as sensed by satellite overnight on 14–15 June 2011 (Figure 7a). There is an approximately 1°C increase above adjacent waters. During a daytime pass on 22 June, the wake waters are over 2°C warmer (Figure 7b). The warmer waters extend over 50 km in the downwind direction and 50 km in width. The same magnitude of warming above background and lateral (–17.5°W to −17°W) and downwind (to 32°N) extension is found in the daytime averaged model fields for 14 and 15 June 2011 (Figure 8). Stronger downwind warming occurs on 15 June on the western portion of the lee-side, while cooler temperatures (relative to the previous day) dominate immediately adjacent to the coast and the eastern side. Lateral variations in daily averaged temperature from 14 to 15 June exceed 1°C.

Anomalously cold ocean temperatures to the southeast of Madeira in the model are linked to a cyclonic oceanic eddy (not shown). The ocean currents are from the north/northwest at this time, which provide a forcing mechanism for oceanic lee eddies to the south [*Arístegui et al*., 1997]. Oceanic cold pools in this region are typically found [*Caldeira et al*., 2002], along with fields of oceanic eddies in the vicinity of Madeira [*Caldeira et al*., 2014]. Satellite altimetry indicates cyclonic circulation in this region in June (not shown). There appears to be a shift in the eddy position from 14 to 15 June and subsequent alignment with the wind-wake, a process termed "eddy-confinement" by *Couvelard et al*. [2012].

In the model, warmer ocean temperatures of 21–23°C are confined to the upper 10 m of the ocean in the meridional cross section at −17.3°W at 18 UTC on 14 June (Figure 9, left). Overnight the near-surface warm waters dissipate (cool) and the warm wake region contracts by about half in north-south extent (to 25 km). The temperatures remain 0.5–1.0°C above adjacent waters in this area. The pattern of diurnal warming is found throughout the time period of the simulation, but its magnitude varies. On 18–19 June (Figure 9, right) the warming is deeper and stronger. Likewise the spatial position of the lee warming is subject to variability (Figure 8). Both are influenced by air-sea interaction processes, as detailed next.

3.3. Drainage Flows

On the night of 15 June a nocturnal drainage flow develops in the model, driving cold air down-valleys and out to sea. Upward sensible heat fluxes reach 50 W/m^2 in the lee of Madeira with strongest fluxes occurring at 06 UTC (Figure 10). By 09 UTC the drainage winds terminate and the downward sensible heat fluxes on the flanks of Madeira attain ∼25 W/m^2 into the ocean. At this time, the downward surface sensible heat fluxes are greater and cover a larger area on the eastern end of Madeira (over a cold SST region) relative to the west side (see Figure 8 for the SST distribution).

Overnight the latent heat fluxes increase in several fingers emanating from the southern coastline and along the wake flanks flowing from the coast, corresponding to the regions of increased winds and surface sensible heat flux (Figure 10). The latent heat fluxes are upward, with the largest latent heat fluxes occurring at 06 UTC (up to 300 W/m^2). By 09 UTC the drainage winds have subsided, but elevated latent heat fluxes (∼15–200 W/m^2) continue on the flanks of the island—indicative of a high moisture flux from the water.

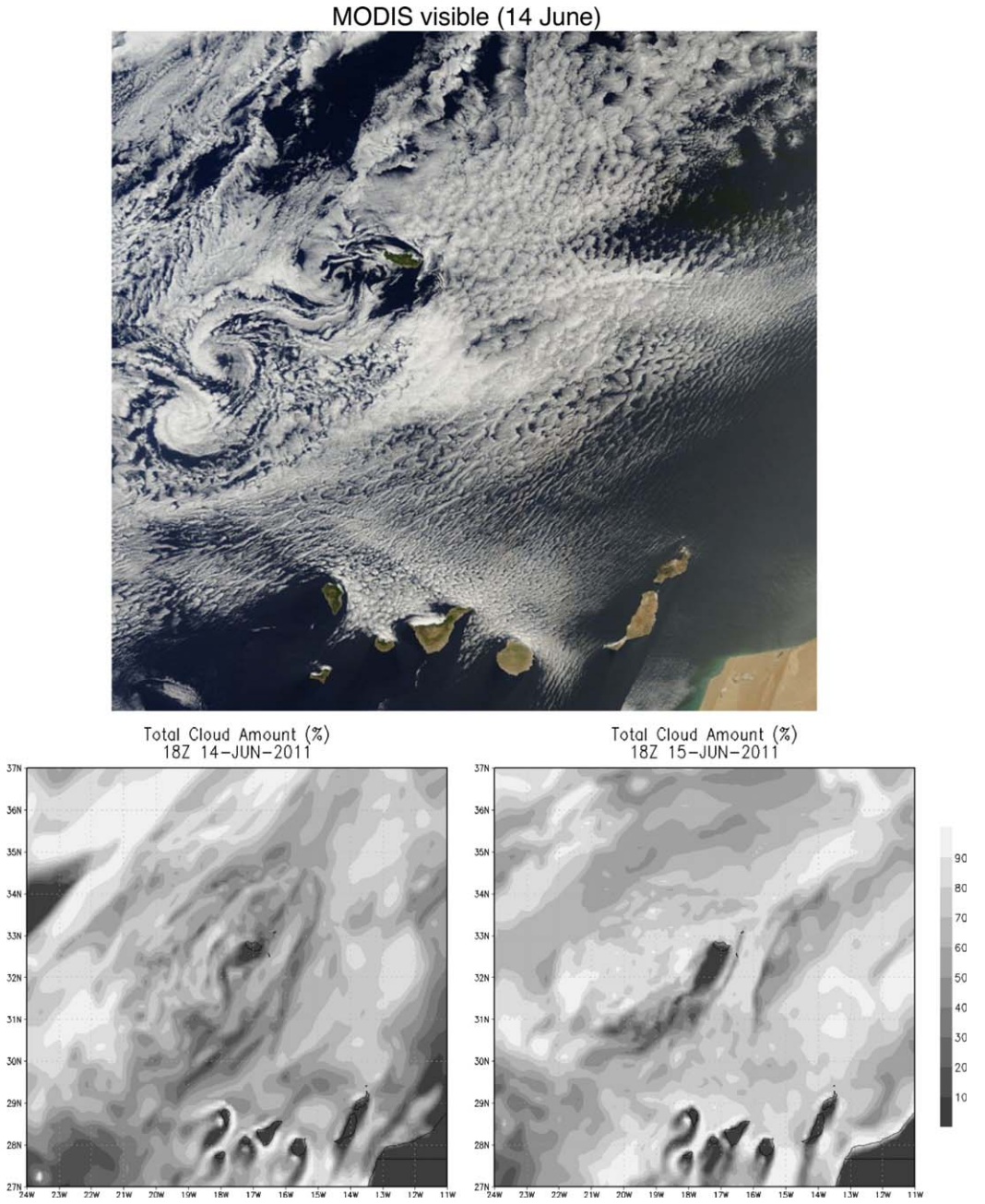

Figure 5. (top) Atmospheric wake in the lee of Madeira Island as imaged by MODIS on 14 June 2011. (bottom) Total cloud amount percentage from the model for 14 and 15 June 2011.

Latent heat fluxes off the east flank of Madeira are more pronounced than the sensible heat fluxes there and extend over 200 km downwind. At the flanks of the islands the orographically dominated "large-scale" winds control latent heat fluxes.

The lee region is examined in more detail for this event (Figure 11, top). Areas of highest wind speed at 06 UTC on the edges of Madeira correspond to diverted flow (tip or flank jets) joined by drainage and/or land breezes. On the southern coast, drainage jets of 7–14 m/s are separated by relatively calmer winds (under 5 m/s). The three coastal areas with highest winds correspond to the deepest ravines on the leeside of Madeira island: Ponta Do Sol to the west (–17.1°W), Ribeira Brava (–17.06°W), and Camara De Lobos to the east (–16.97°W).

Although other southern coastal sites did not measure wind (Ponta do Sol) and/or were clearly blocked by terrain in their siting (Quinta Grande), there is some signature of downslope winds at the Funchal Lido

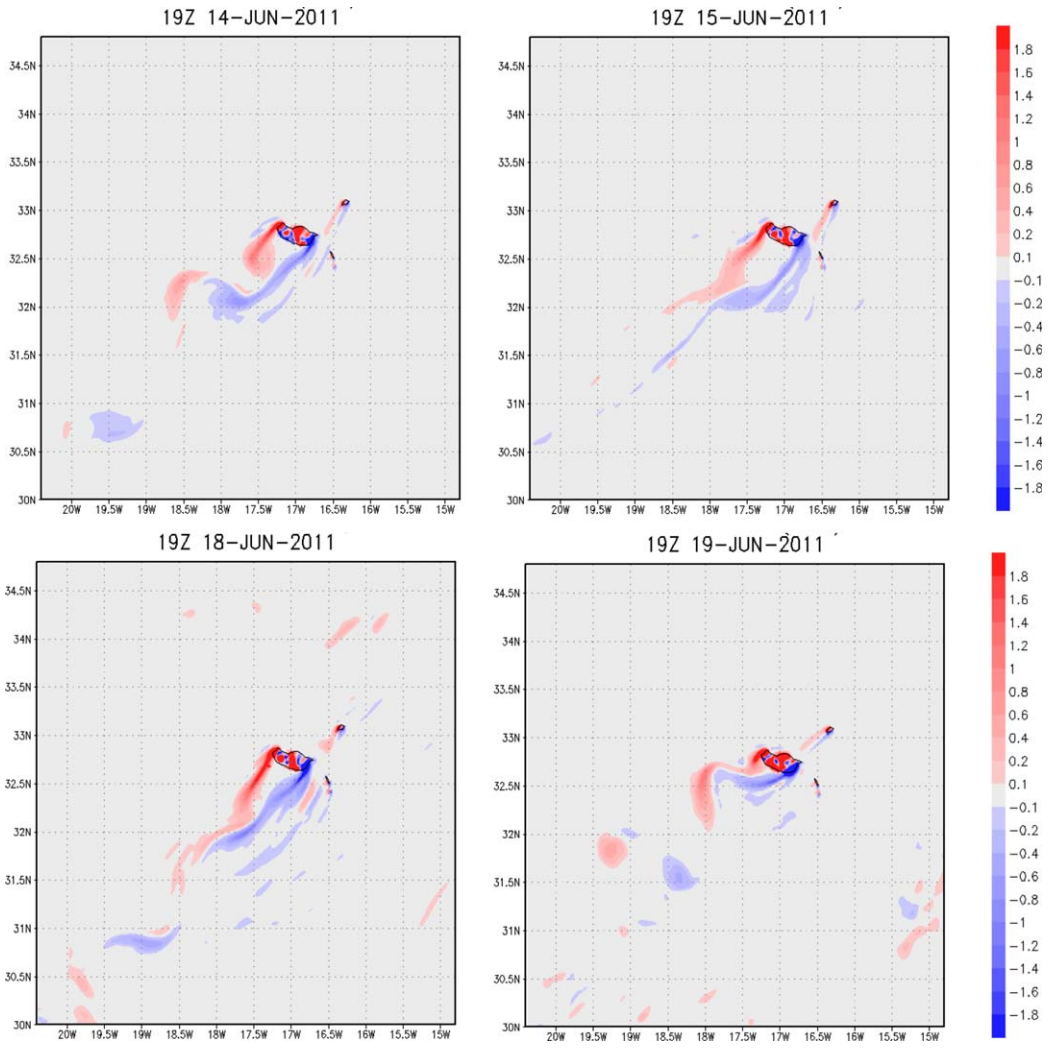

Figure 6. Wind stress curl (units of $\times 10^{-5}$ N/m^2) during early evening for several days of the simulation. These consist of (top left) 14 June strong wake, (top right) 15 June weak wake, (bottom left) 18 June weak wake, and (bottom right) 19 June strong wake.

station (Figure 11, bottom). It is likely that the station at 25 m elevation adjacent to Madeira's main city is not optimally sited. Nonetheless there is a suggestion of down-valley winds on the morning of 15 June, albeit weaker by a factor of 2–3 than the model-derived values that were extracted at the same latitude/longitude corresponding to a model elevation of 68 m. Locally, across the island the drainage winds are recognized as prevalent features that are revealed in photos showing fog near ground level rushing down the valleys (R. Caldeira, personal communication, 2016).

The model wind is strong (10 m/s) and cold (~19°C) at the western lee site (–17.2°W, 32.68°N, red line, whose location is shown in Figure 11 by a red star) in the early morning hours of 15 June (Figure 12). At the western lee location, the underlying SST is ~21°C during the drainage event. The total upward heat flux peaks at 250 W/m^2. The short wave radiation on 15 June is only marginally greater than on 14 June at this location, but leads to an equilibration in the air and sea temperatures by noon on 15 June (and much reduced surface heat fluxes). In this persistent wake region, SSTs show increased upward progression with repeated diurnal warming episodes (red line).

Strong, cool down-ravine winds also occur on the mornings of 11, 12, 14, and 18 June, but at reduced magnitude relative to the 15 June event (Figure 12). At the central site located offshore in the down-valley wind footprint (black line) the episodic cooling from these other events is more pronounced, particularly early in the record. The progressive diurnal SST warming is less evident relative to the western site.

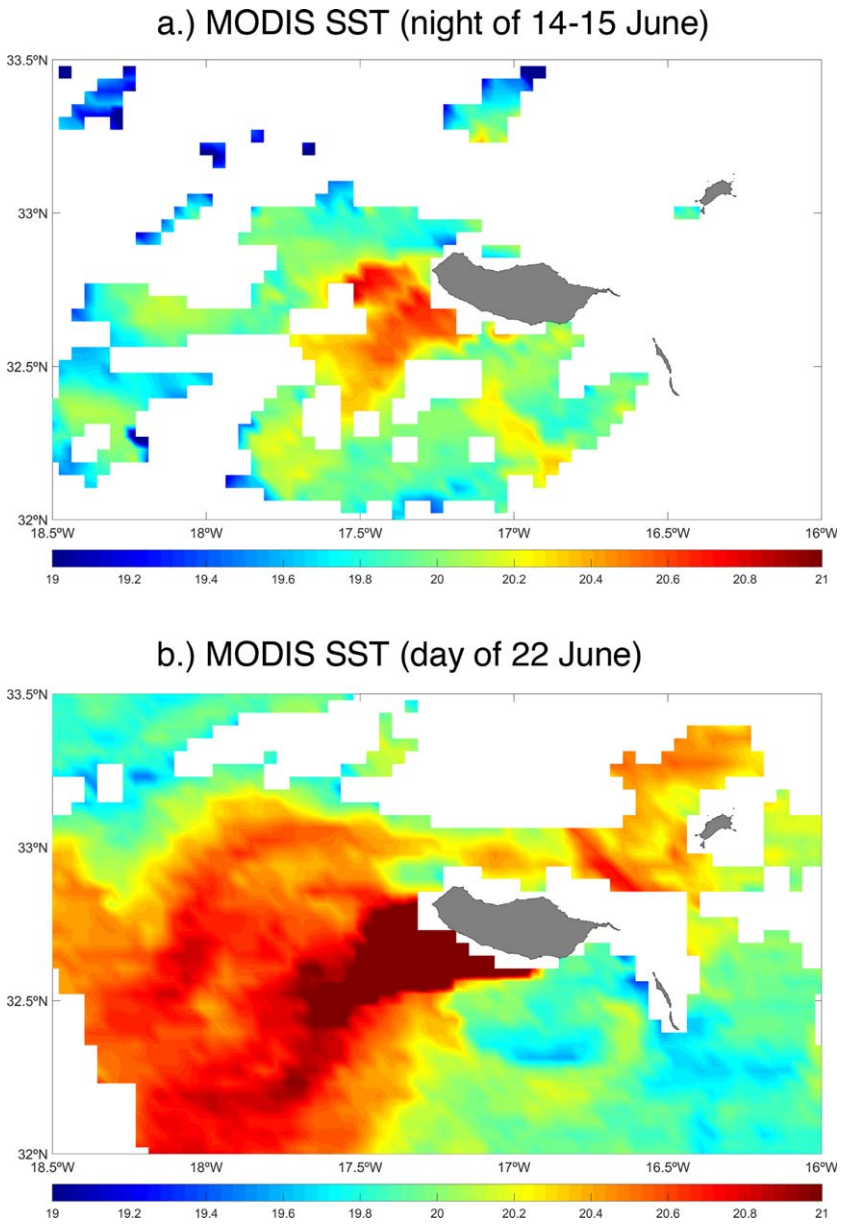

Figure 7. Warming in the lee of Madeira from MODIS Aqua L3 SST overpass at 4 km resolution on partially cloud-free (a) overnight of 14–15 June 2011 and (b) day of 22 June 2011. Units are °C.

Strong winds at the site at the eastern periphery of the lee region overlay cooler SSTs (blue line) and a muted diurnal cycle (Figure 12). There the cold air drainage flow on the eastern end of Madeira appears to join the flank wind jet on 15 June. And elevated latent heat fluxes generally occur during the windy period after 15 June.

At all sites there is reduced diurnal warming on 12 and 16 June during those lower insolation days. However, a direct relationship between SST and cloudiness is not always evident, and the atmospheric wake can frequently display a very detailed evolution both temporally and spatially. SST also depends on the presence of oceanic eddies as well as general ocean advection patterns.

We can examine the relationship between SST and latent and sensible heat fluxes under the 15 June drainage winds by comparing with a case on 18–19 June without drainage flow that displays a weak-to-strong atmospheric wake transition. The overnight SST difference of 14–15 June versus 18–19 June shows more cooling in the ∼30 km lee zone offshore of Madeira overnight during the 15 June drainage wind event

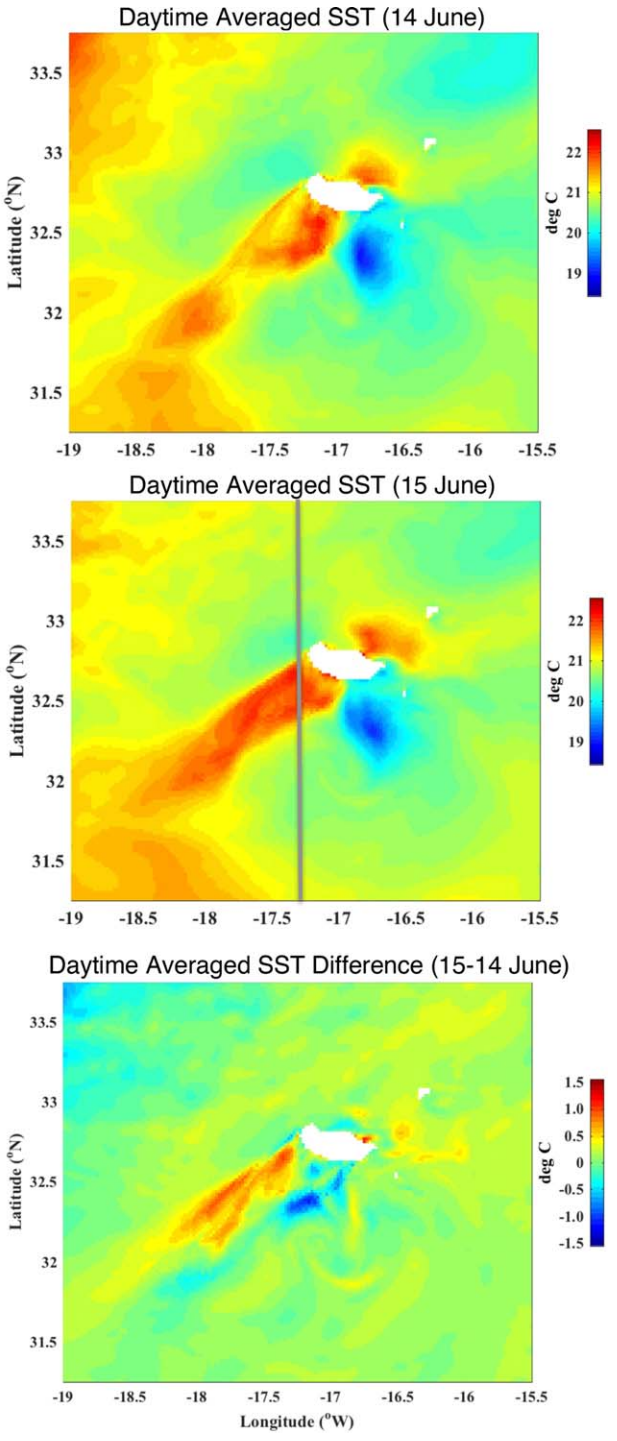

Figure 8. Average of SST on (top) 14 and 15 June 2011 daytime (06 UTC to 18 UTC) using 3-hourly fields and (bottom) 15 June minus 14 June. The meridional transect location at −17.3°W of Figure 9 is indicated in the middle plot.

(Figure 13). SST change is doubled (overnight difference from 1.5°C to 3°C colder) in some areas. The difference between overnight of 15 June and overnight of 19 June (Figure 13, bottom) shows slight to strong cooling in the downwind region, with most change occurring on the western flank related to the positional variation of the warm wake.

3.4. Atmosphere and Ocean Boundary Layer Interaction

Down-ravine flows of cold mountain air erode the warm temperature signature in the ocean overnight and enhance sea surface mixing (Figure 14). The zonal cross section at 32.5°N reveals near-surface cooling and slight ocean surface mixed layer deepening (by ∼5 m) at ∼17.2°W under the cold air prong at 06 UTC 15 June. The transect captures two of the drainage wind flows emanating from Ribeira Brava and Camara De Lobos valleys. The western-most drainage flow is deflected at this latitude and barely appears in the section. However, the colder air on each side of Madeira is captured in the transect, and is present at earlier and later times (18 UTC on 14 and 15 June).

On 15 June at 18 UTC, strong ocean warming is apparent near the surface (Figure 14). It is concentrated to the west relative to the day before, as was also illustrated in the SST distribution (Figure 8). The leeside warming correlates with high air temperatures (∼20.5°C) above the warm wake at this early evening time. The contraction of the lee side warm region overnight and reformation the subsequent day is associated with enhanced atmospheric warming under relatively cloud-free conditions (Figure 5), and mutual adjustment between the boundary layers.

The Madeira overnight drainage flow cools and stratifies the lower ABL relative to the previous night, as seen in a diagonal transect aligned with the wind and crossing through high terrain (Figure 15: 06 UTC 15 June relative to 18 UTC 14 June). The ability for the ABL to warm in response to the diurnally heated SST in the cloud-free wake is compromised the next day (15 June) following the nocturnal down-valley cold air event. Consequently the ABL height is shallower by ∼200–500 m compared with the previous day (14 June).

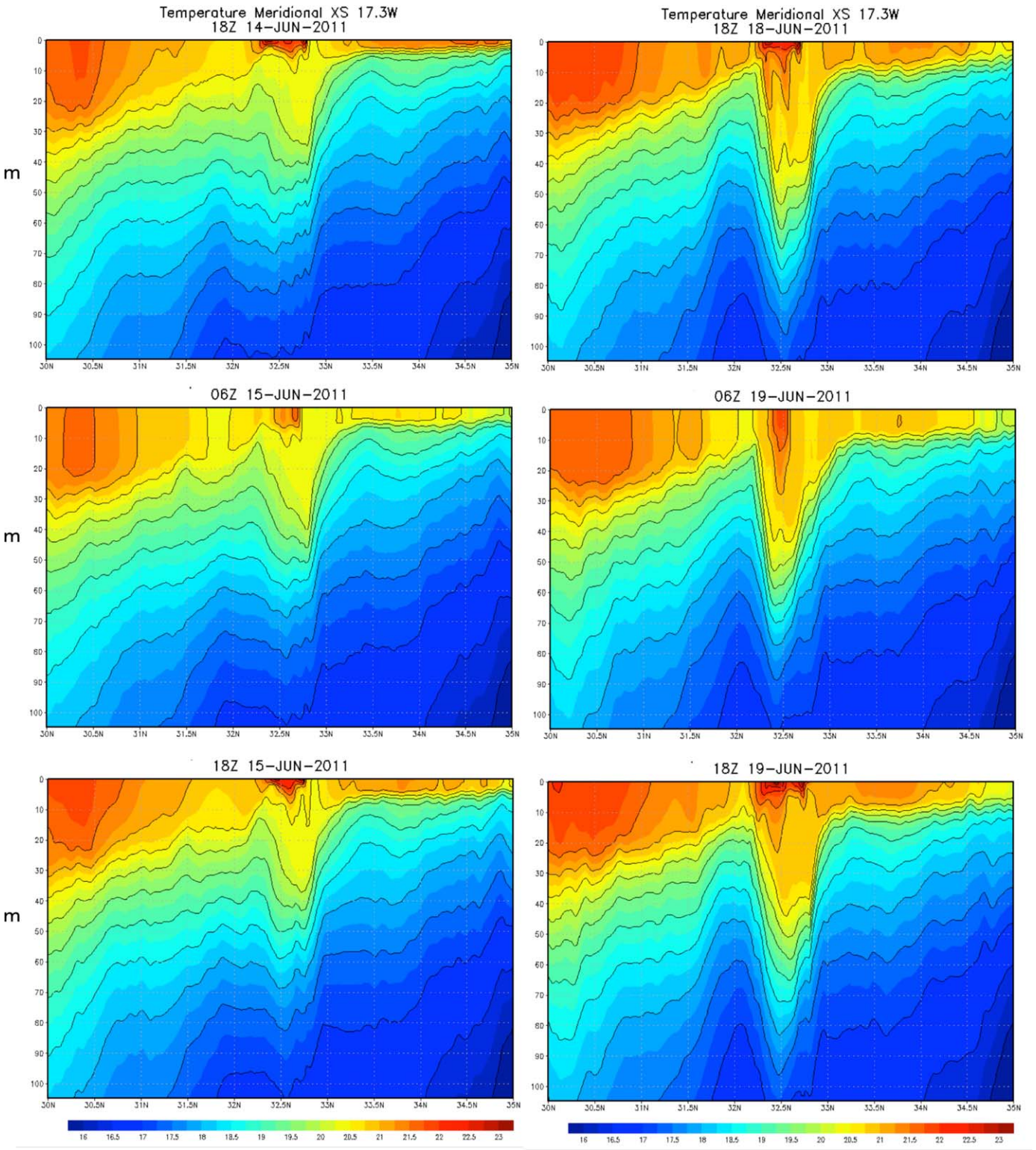

Figure 9. Diurnal evolution of ocean temperature in the model along the meridional transect at −17.3°W (shown in Figure 8) from (left) 14 to 15 June 2011 and (right) 18 to 19 June. Units are °C.

To examine more closely the impact of the two-way coupling, two additional numerical simulations were conducted. They both utilize the same configuration as described previously, but are initialized on 00 UTC 12 June and run through 15 June (96 h). The uncoupled run uses analyzed SST from NCODA, updated at a 12 h frequency; the coupled run employs the coupled model as detailed in section 2. The

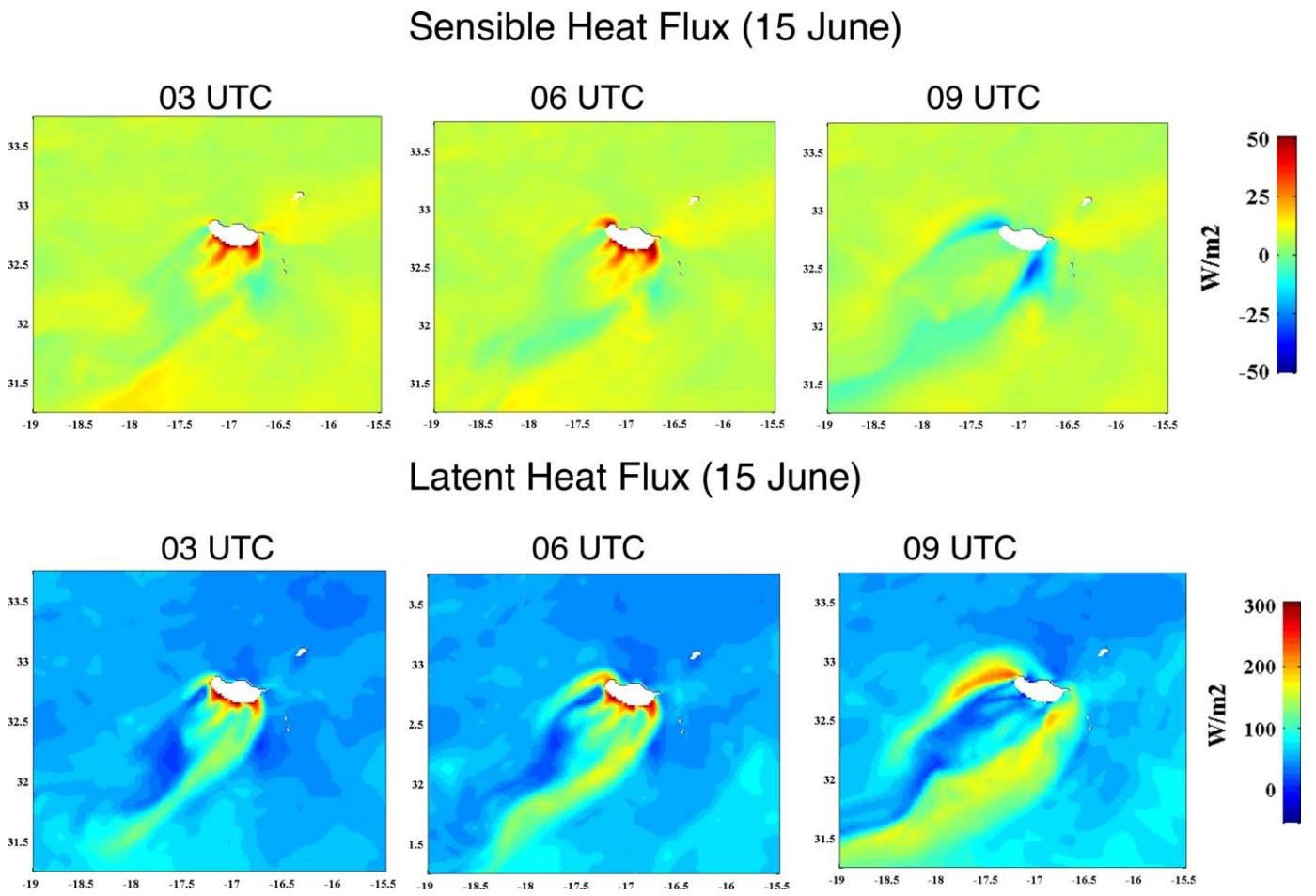

Figure 10. Modeled (top) sensible and (bottom) latent heat flux for several hours of 15 June 2011.

uncoupled run is meant to mimic the treatment of the ocean that is often used in atmosphere-only simulations.

The impact of the coupling is evident throughout the short sensitivity simulation. The near-surface air temperature difference is ~3°C in the late afternoon (18 UTC June 14) and around 1–2°C at night and early morning (06 UTC 14 June) (Figure 16). Therefore the warmer air temperatures in the coupled run relative to the uncoupled run are persistent and are most pronounced in the wake region. In the lee, latent heat fluxes are 100–150 W/m^2 stronger on 18 UTC 14 June for the coupled run (Figure 17, top). These heat flux differences are driven by underlying SST differences of 2–3°C in the island lee (Figure 17, bottom).

In the vertical, warmer air temperatures in the lee extend over a depth of 500 m in the coupled run compared with the uncoupled run (Figure 18). There is also evidence of warmer temperatures above the atmospheric boundary layer in the 1–2.5 km layer. The sensitivity run highlights the impact within and above the atmospheric boundary layer due to increased interactive surface oceanic warming in the lee of the island on a diurnal basis.

4. Summary and Discussion

A study was undertaken to explore the impact of processes not included in uncoupled or coarse resolution (e.g., global or some regional) simulations. To our knowledge, this is the first examination of the coupled air/sea boundary layer response in an island lee-side warm wake. In addition, the representation and quantification of drainage flow interaction with the coastal ocean is a unique aspect of our study.

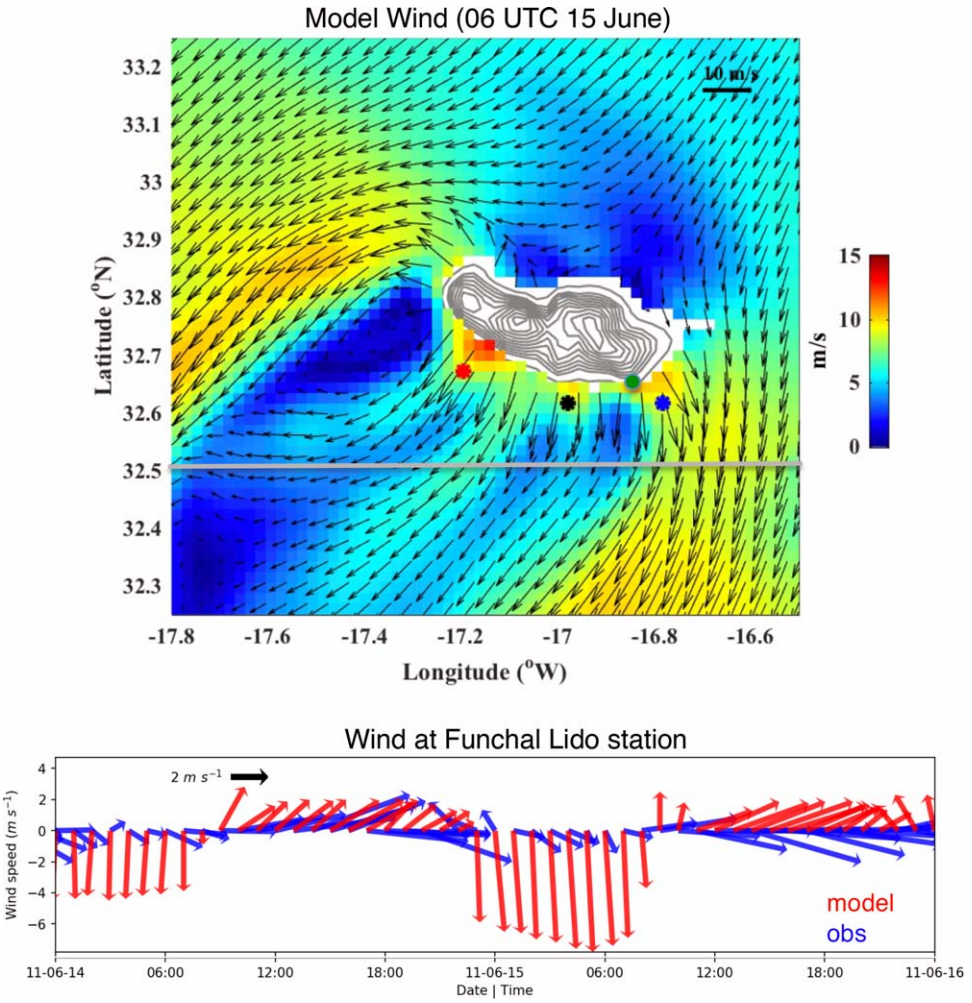

Figure 11. (top) The 06 UTC 15 June wind speed and direction. The lee locations for the time series in Figure 12 are shown with stars, and Funchal Lido station is indicated with a green circle. The western(red)/central(black)/eastern(blue) lee points are located at ocean depths of 526, 165, and 289 m, respectively. The terrain is shown at 100 m contours above 500 m, with a maximum of 1400 m. The zonal section at 32.5°N used in Figure 14 is indicated. (bottom) Observed and modeled winds at Funchal Lido station.

To summarize, satellite imagery of Madeira Island showed atmospheric vortex shedding (strong wake) occurring on 14 June 2011, concurrent with the formation of a lee warm oceanic wake. These conditions were reproduced in the high-resolution two-way coupled model configured for Madeira. On 15 June, the wake shifted to a weak regime (no vortex shedding) in the model. We contrast this case with a weak to strong atmospheric wake transition on 18–19 June 2011.

The model SST variations around Madeira (eddies, fronts) were supported by prior local and regional field studies, as well as satellite imagery. COAMPS sea level pressure, air-temperature and winds compared well with in situ meteorological observations at 14 sites for the simulation time period in June 2011. Specifically, RMSE and bias values were at acceptable levels. Sites in more complex terrain produced weaker model-data comparisons. As found previously, instrument sites on Madeira's rugged terrain are rarely representative of nearby areas, and are commonly subjected to very local flow fields [*Palma et al.*, 2008].

The model-derived diurnal cycle showed warm wake formation (2°C, impacting the upper 20 m) maintained during daytime and insulated by a lower ABL topped at ~300 m on 15 June. Down-ravine winds contributed to the nighttime dissipation of the warm sea surface wake. In their presence, intense atmospheric heat fluxes (~300 W/m^2) can occur leeward of ravines. These high upward heat fluxes extend out to about 30 km offshore during the early morning hours in the model. The 15 June event is contrasted with the situation on 19 June in the absence of drainage winds. Greater and deeper near-surface ocean warming occurs

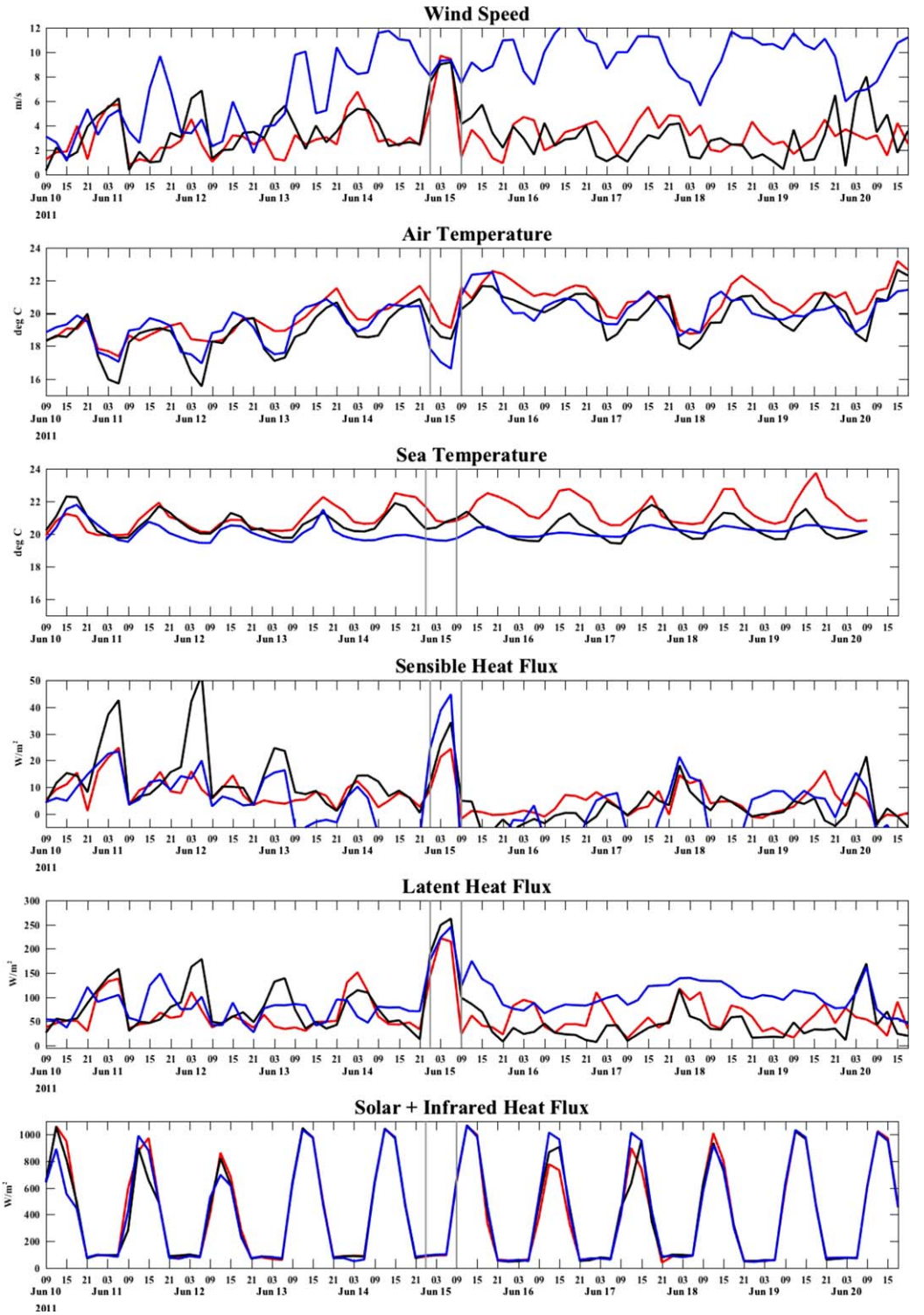

Figure 12. Time series for 10–20 June of model 10 m wind speed, 2 m air temperature, SST and heat fluxes at the locations marked in Figure 11. The western/central/eastern lee sites are denoted by red, black, and blue lines, respectively. The period of strong drainage winds on 15 June is delineated with grey bars.

during 18–19 June, and the magnitude of overnight/morning cooling is reduced. Therefore drainage flows can erode the warm wake and augment nocturnal erosion already present due to the absence of solar heating. Nevertheless, the upper ocean stores some heat overnight as a "memory" imprinted on the oceanic boundary layer. This overnight warm wake maintenance amounts to ~1°C in the upper 5 m and was

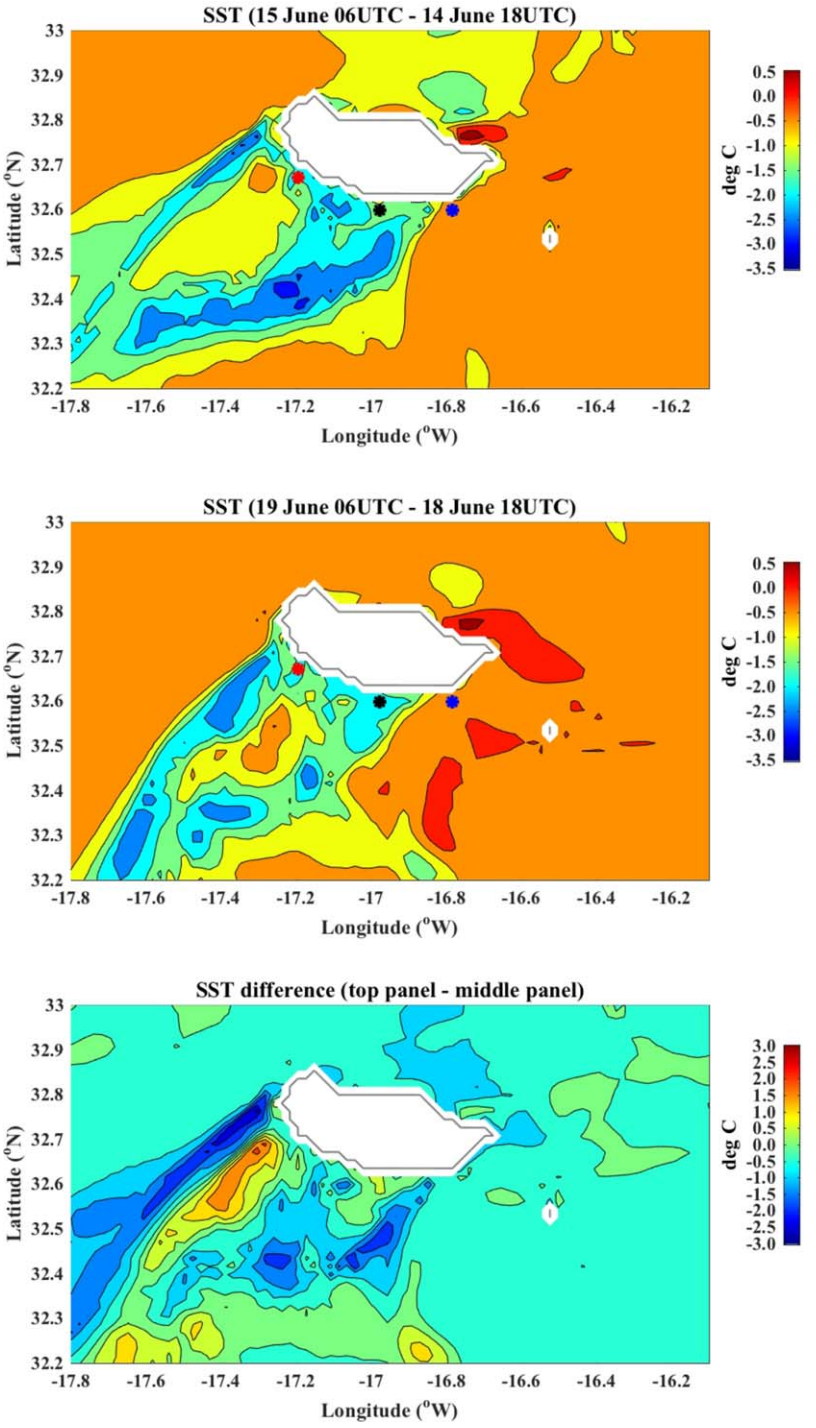

Figure 13. Overnight erosion of warm SST in the lee region on (top) 15 June and (middle) 19 June. Differences between 06 UTC and the prior day 18 UTC are shown. The western(red)/central(black)/eastern(blue) lee locations used for the timeseries of Figure 11 are indicated. The bottom plot shows the top minus the middle, i.e., the difference of overnight differences. Contour intervals are 0.5°C.

confirmed by satellite remote sensing. In the model, the progressive accumulation of diurnal warming was notable under the persistent wake relative to other island lee locations.

The strong winds on the flanks of Madeira Island in the tip jets control the large-scale latent heat fluxes. The drainage winds occur on an episodic basis leading to large upward heat fluxes at offshore locations in the

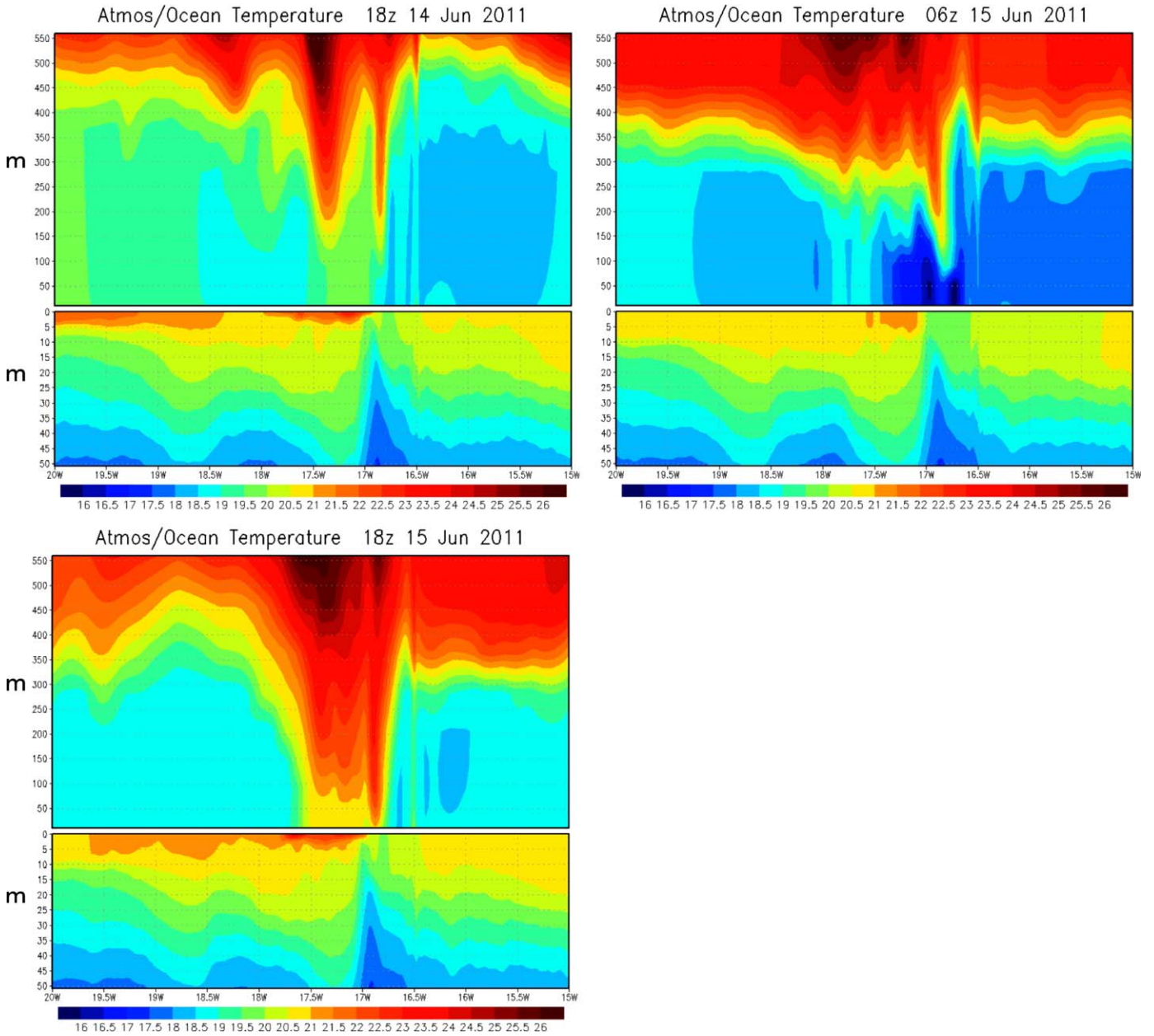

Figure 14. Atmosphere and ocean temperature cross section for several times on 14–15 June 2011 along zonal section at 32.5°N (shown in Figure 11).

lee. The drainage winds in our simulation are reminiscent of coastal katabatic winds identified by SAR off California and Oregon [*Li et al*., 2007]. There, the wind speeds were 5–8 m/s and extended over 20 km offshore. These characteristics are comparable to the winds described here.

In a set of sensitivity runs designed to examine the impact of two-way coupling on the ABL, near-surface air temperatures were 1–3°C warmer throughout the simulation in the coupled run relative to the uncoupled run. In the coupled run, temperatures were warmer in the lower >500 m of the ABL as a result of the increased surface heat fluxes in the lee region. Our results are in general agreement with the magnitude of changes induced by SST fronts on the ABL. For example, sensible (latent) heat fluxes of 30–50 W/m^2 (150 W/m^2) are found in response to several degree SST gradients in studied regions [*Small et al*., 2008]. Adjustments of ABL height of several hundred meters are expected in the wake area of Madeira based on the results of *Grubišić et al*. [2015]. And prior COAMPS simulations for downslope bora windstorms in the

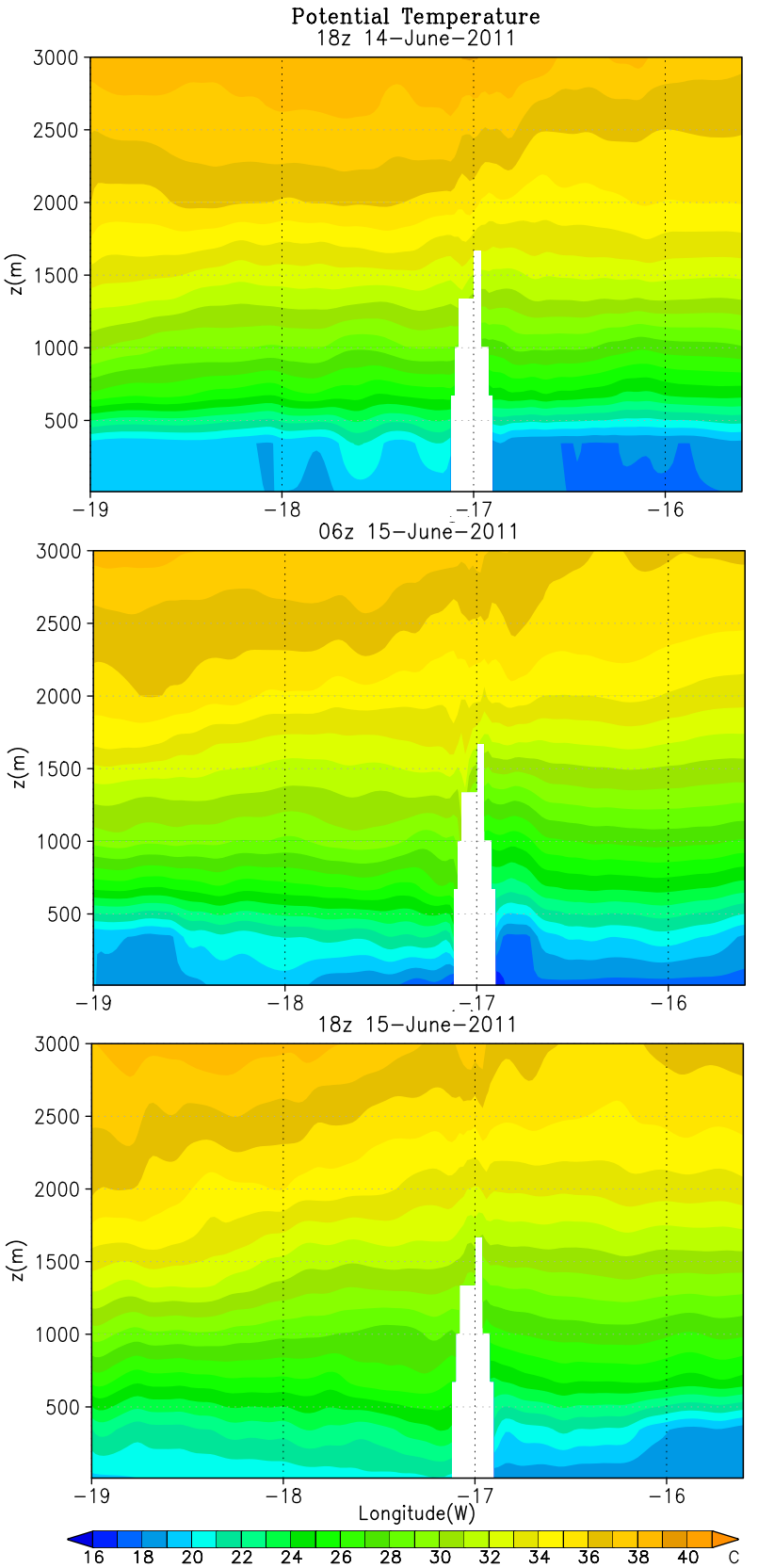

Figure 15. Atmosphere potential temperature cross section at several hours through the middle portion of the island along the direction of the wind from southwest to northeast, anchored at (31°N, 19°W) to (34°N, 15.6°W).

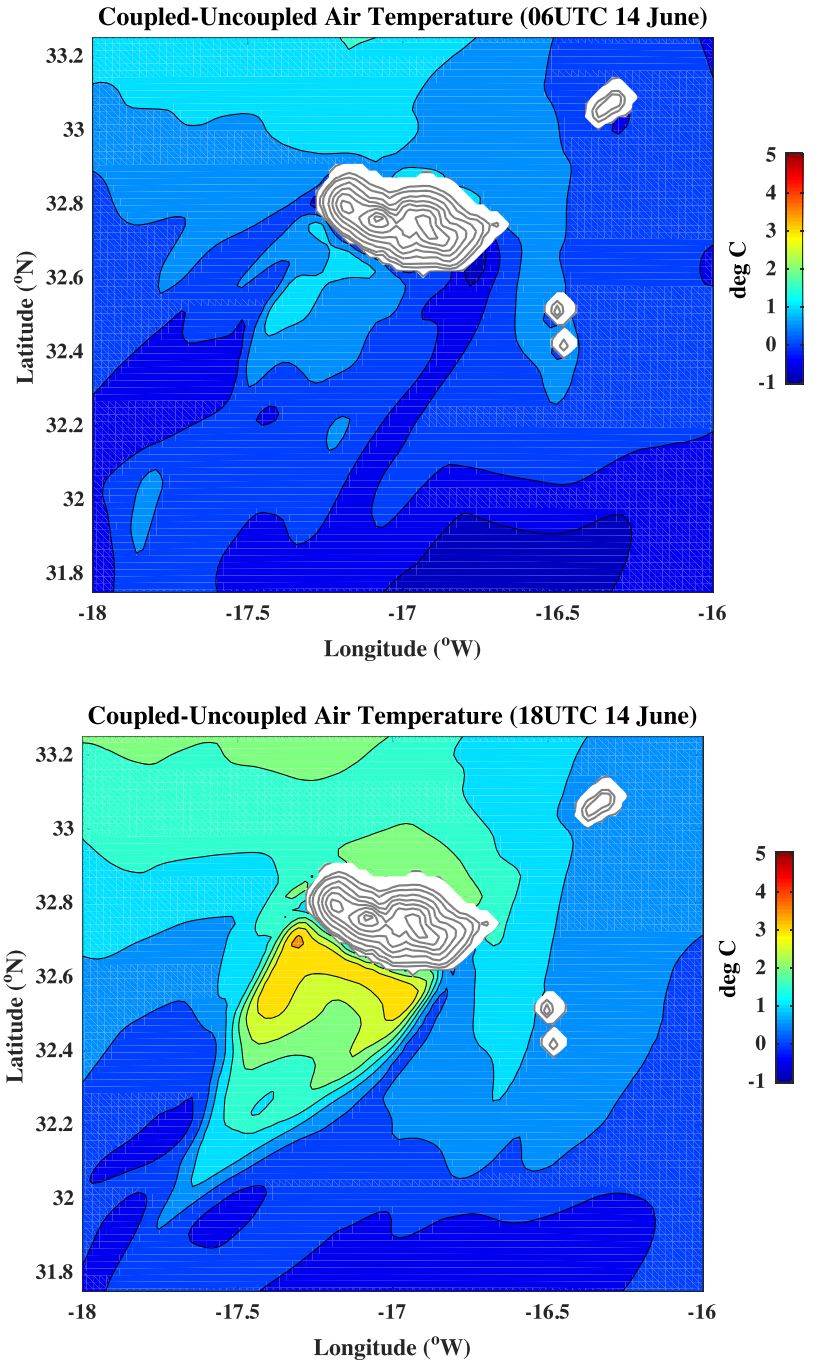

Figure 16. Difference between coupled and uncoupled simulated 2 m air temperature in (top) the morning and (bottom) late afternoon of 14 June. Contour intervals are 0.5°C. Terrain is shown at 50, 100, and a 250 m interval thereafter.

Adriatic produced superior heat fluxes in two-way coupled mode compared with uncoupled results, increasing the correspondence of the model results in relation to observations [*Pullen et al*., 2007].

However, atmospheric flows over and around complex terrain remain challenging to simulate with high fidelity [*Doyle et al*., 2013]. Though the downslope flow is suggested by limited coastal measurements, it is likely that the model overestimates the drainage winds and surface heat fluxes. In the case of New Caledonia, too strong drainage flow was attributed to weak surface roughness in the model [*Lefèvre et al*., 2010]. And urban features have been shown to modify katabatic winds through warming from anthropogenic sources [*Lee and Kim*, 2010]. Field studies are needed to measure the dynamics in the warm wake

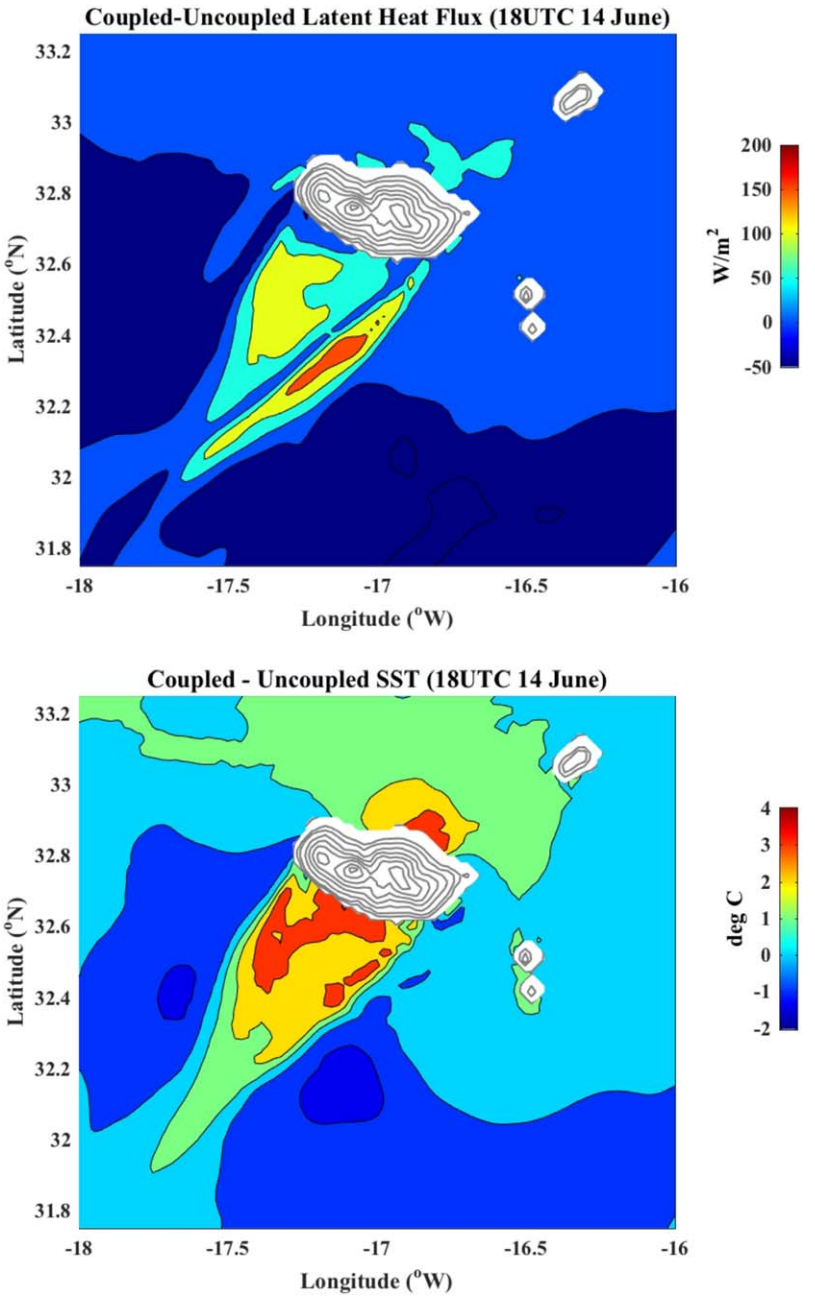

Figure 17. (top) Difference between coupled and uncoupled simulated latent heat flux in the late afternoon of 14 June. Contour intervals are 50 W/m^2. (bottom) Difference between coupled and uncoupled simulated SST for the same time. Contour intervals are 1°C. Terrain is shown at 50, 100, and a 250 m interval thereafter.

region and specifically to quantify the fluxes during drainage winds that occur intermittently in the early morning hours.

Wake regimes are frequently categorized in a static manner that belies more energetic fluctuations unique to island environments [*Isoguchi et al.,* 2010]. Recent LES simulations of vortex shedding in a convective boundary layer highlight the role of surface fluxes in facilitating vortex decay away from the island [*Heinze et al.*, 2012]. These studies along with ours motivate the need for a systematic examination of the role of ABL characteristics such as inversion strength, and downwind air/sea processes in shifting between strong and weak wake events in realistic cases, as suggested by *Caldeira and Tomé* [2013].

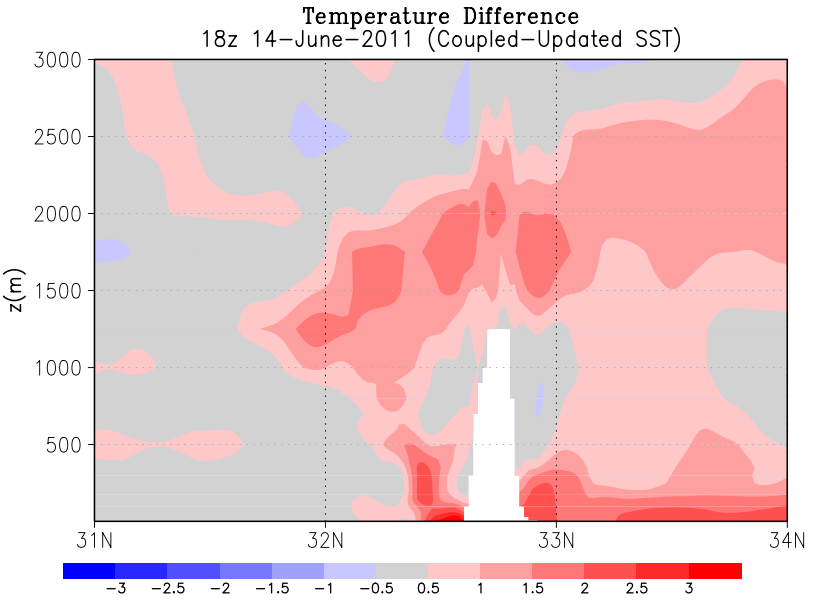

Figure 18. Potential temperature difference (°C) between the coupled and uncoupled (that uses updated analyzed SST) simulations in the late afternoon of 14 June on a meridional transect through −17°W.

Microclimates encompassing small scales render Madeira's surface highly heterogeneous. Thus, higher-resolution model implementations are desired to better resolve the terrain and land surface at <2 km. Madeira also experiences significant rainfall-induced flooding due to orographic precipitation [*Couto et al.*, 2012], further motivating the utilization of a comprehensive coupled earth system model.

An urban canopy parameterization [*Holt and Pullen*, 2007] and advanced land surface and hydrology model components (WRF-Hydro and NASA's Land Information System) are recent additions to the COAMPS system (T. Holt, personal communication, 2016). Future simulations of Madeira Island will include more comprehensive, and higher-resolution, treatment of the land surface-hydrology-urban linkages to improve hazard prediction.

Acknowledgments

Data utilized in this research are available at doi:10.1594/PANGAEA.875975. COAMPS® is a registered trademark of the Naval Research Laboratory. J. Pullen acknowledges the support of Office of Naval Research (ONR) grant N00014–10-1–0300. Rui Caldeira is funded by Project "Observatório Oceânico da Madeira- OOM" (M1420–01-0145-FEDER-000001), co-financed by the Madeira Regional Operational Programme (Madeira 14–20), under the Portugal 2020 strategy, through the European Regional Development Fund (ERDF). J. Doyle and P. May were supported by ONR program elements (PEs) 0601153N and 0602435N and the Chief of Naval Research through the NRL Base Program, PE 0601153N. The meteorological station data were kindly provided by Vitor Prior from the Madeira delegation of IPMA—Instituto Português do Mar e da Atmosfera. We are thankful to two anonymous reviewers whose feedback and queries improved the quality of the manuscript.

References

Allard, R. A., et al. (2010), Validation test report for the coupled ocean/atmosphere mesoscale prediction system (COAMPS) version 5.0, *Rep. NRL/MR/7320–10–9283*, Naval Res. Lab, Stennis Space Cent., MS Oceanogr. Div., Miss.

Alpers, W., U. Pahl, and G. Gross (1998), Katabatic wind fields in coastal areas studied by ERS-1 synthetic aperture radar imagery and numerical modeling, *J. Geophys. Res.*, *103*(C4), 7875–7886.

Arístegui, J., et al. (1997), The influence of island-generated eddies on chlorophyll distribution: a study of mesoscale variation around Gran Canaria, *Deep Sea Res., Part I*, *44*(1), 71–96.

Barron, C. N., A. B. Kara, P. J. Martin, R. C. Rhodes, and L. F. Smedstad (2006), Formulation, implementation and examination of vertical coordinate choices in the Global Navy Coastal Ocean Model (NCOM), *Ocean Modell.*, *11*(3), 347–375.

Barton, E. D., G. Basterretxea, P. Flament, E. G. Mitchelson-Jacob, B. Jones, J. Arístegui, and F. Herrera (2000), Lee region of Gran Canaria, *J. Geophys. Res.*, *105*(C7), 17,173–17,193.

Caldeira, R., A. Stegner, X. Couvelard, I. B. Araújo, P. Testor, and A. Lorenzo (2014), Evolution of an oceanic anticyclone in the lee of Madeira Island: In situ and remote sensing survey, *J. Geophys. Res. Oceans*, *119*, 1195–1216, doi:10.1002/2013JC009493.

Caldeira, R., X. Couvelard, R. Vieira, C. Lucas, I. Sala, and I. Vallès Casanova (2016), Challenges of building an operational ocean forecasting system for small island regions: Regional to local, *J. Oper. Oceanogr.*, *9*, 1–12.

Caldeira, R. M., and R. Tomé (2013), Wake response to an ocean-feedback mechanism: Madeira Island case study, *Boundary Layer Meteorol.*, *148*(2), 419–436.

Caldeira, R. M. A., and P. Marchesiello (2002), Ocean response to wind sheltering in the Southern California Bight, *Geophys. Res. Lett.*, *29*(13), doi:10.1029/2001GL014563.

Caldeira, R. M. A., S. Groom, P. Miller, D. Pilgrim, and N. P. Nezlin (2002), Sea-surface signatures of the island mass effect phenomena around Madeira Island, Northeast Atlantic, *Remote Sens. Environ.*, *80*(2), 336–360.

Cécé, R., D. Bernard, C. d'Alexis, and J. F. Dorville (2014), Numerical simulations of island-induced circulations and windward katabatic flow over the Guadeloupe archipelago, *Mon. Weather Rev.*, *142*(2), 850–867.

Chen, S., T. J. Campbell, H. Jin, S. Gaberšek, R. M. Hodur, and P. Martin (2010), Effect of two-way air-sea coupling in high and low wind speed regimes, *Mon. Weather Rev.*, *138*(9), 3579–3602.

Chopra, K. P., and L. F. Hubert (1965), Mesoscale eddies in wake of islands, *J. Atmos. Sci.*, *22*(6), 652–657.

Couto, F. T., R. Salgado, and M. J. Costa (2012), Analysis of intense rainfall events on Madeira Island during the 2009/2010 winter, *Nat. Hazards Earth Syst. Sci.*, *12*(7), 2225–2240.

Couvelard, X., R. M. A. Caldeira, I. B. Araújo, and R. Tomé (2012), Wind mediated vorticity-generation and eddy-confinement, leeward of the Madeira Island: 2008 numerical case study, *Dyn. Atmos. Oceans*, *58*, 128–149.
Cummings, J. A. (2005), Operational multivariate ocean data assimilation, *Q. J. R. Meteorol. Soc., Part C*, *131*(613), 3583–3604.
Cuxart, J., M. A. Jiménez, and D. Martínez (2007), Nocturnal meso-beta basin and katabatic flows on a midlatitude island, *Mon. Weather Rev.*, *135*(3), 918–932.
Daley, R., and E. Barker (2001), NAVDAS: Formulation and diagnostics, *Mon. Weather Rev.*, *129*(4), 869–883.
Doyle, J. D., and M. A. Shapiro (1999), Flow response to large-scale topography: The Greenland tip jet, *Tellus, Ser. A*, *51*, 728–748.
Doyle, J. D., V. Grubišic, W. O. Brown, S. F. De Wekker, A. Dörnbrack, Q. Jiang, S. Mayor, and M. Weissmann (2009), Observations and numerical simulations of subrotor vortices during T-REX, *J. Atmos. Sci.*, *66*(5), 1229–1249.
Doyle, J. D., Q. Jiang, R. B. Smith, and V. Grubišić (2011), Three-dimensional characteristics of stratospheric mountain waves during T-REX, *Mon. Weather Rev.*, *139*, 3–23.
Doyle, J. D., C. C. Epifanio, A. Persson, P. A. Reinecke, and G. Zängl (2013), Mesoscale modeling over complex terrain: numerical and predictability perspectives, in *Mountain Weather Research and Forecasting*, pp. 531–589, Springer, Dordrecht, Netherlands.
Etling, D. (1989), On atmospheric vortex streets in the wake of large islands, *Meteorol. Atmos. Phys.*, *41*, 147–164.
Fairall, C.W., E. F. Bradley, J. E. Hare, A. A. Grachev and J. B. Edson (2003), Bulk parameterization of air–sea fluxes: Updates and verification for the COARE algorithm, *J. Clim.*, *16*(4), 571–591.
Feng, J., and Y. L. Chen (2001), Numerical simulations of airflow and cloud distributions over the windward side of the Island of Hawaii. Part II: Nocturnal flow regime, *Mon. Weather Rev.*, *129*(5), 1135–1147.
Fu, Q., and K.-N. Liou (1992), On the correlated k-distribution method for radiative transfer in nonhomogenous atmospheres, *J. Atmos. Sci.*, *49*, 2139–2156.
Galvin, J. F. P. (2015), Nocturnal mountain winds in Cyprus—An observational study, *Meteorol. Appl.*, *22*(3), 348–359.
Gille, S. T., S. G. Llewellyn Smith, and N. M. Statom (2005), Global observations of the land breeze, *Geophys. Res. Lett.*, *32*, L05605, doi: 10.1029/2004GL022139.
Grubišić, V., J. Sachsperger, and R. M. Caldeira (2015), Atmospheric wake of Madeira: First aerial observations and numerical simulations, *J. Atmos. Sci.*, *72*(12), 4755–4776.
Hafner, J., and S. P. Xie (2003), Far-field simulation of the Hawaiian wake: Sea surface temperature and orographic effects, *J. Atmos. Sci.*, *60*(24), 3021–3032.
Heinze, R., S. Raasch, and D. Etling (2012), The structure of Kármán vortex streets in the atmospheric boundary layer derived from large eddy simulation, *Meteorol. Z.*, *21*(3), 221–237.
Hodur, R. M. (1997), The Naval Research Laboratory's coupled ocean/atmosphere mesoscale prediction system (COAMPS), *Mon. Weather Rev.*, *125*(7), 1414–1430.
Holt, T., and J. Pullen (2007), Urban canopy modeling of the New York City metropolitan area: A comparison and validation of single-layer and multi-layer parameterizations, *Mon. Weather Rev.*, *135*, 1906–1930.
Isoguchi, O., M. Shimada, and H. Kawamura (2010), Characteristics of ocean surface winds in the lee of an isolated island observed by synthetic aperture radar, *Mon. Weather Rev.*, *139*(6), 1744–1761.
Jiang, Q., and J. D. Doyle (2009), The impact of moisture on Mountain Waves, *Mon. Weather Rev.*, *137*, 3888–3906.
Kain, J. S., and J. M. Fritsch (1993), Convective parameterization for mesoscale models: The Kain-Fritsch scheme, in The Representation of Cumulus Convection in Numerical Models, Meteorol. Monogr. Ser., vol. 46, pp. 165–170, Am. Meteorol. Soc., Boston, Md.
Lee, S. H., and H. D. Kim (2010), Modification of nocturnal drainage flow due to urban surface heat flux, *Asia-Pac. J. Atmos. Sci.*, *46*(4), 453–465.
Lefèvre, J., P. Marchesiello, N. C. Jourdain, C. Menkes, and A. Leroy (2010), Weather regimes and orographic circulation around New Caledonia, *Mar. Pollut. Bull.*, *61*(7), 413–431.
Li, X., W. Zheng, W. G. Pichel, C. Z. Zou, and P. Clemente-Colón (2007), Coastal katabatic winds imaged by SAR, *Geophys. Res. Lett.*, *34*, L03804, doi:10.1029/2006GL028055.
Louis, J. F. (1979), A parametric model of vertical eddy fluxes in the atmosphere, *Boundary Layer Meteorol.*, *17*, 187–202.
Martin, P. J. (2000), Description of the NAVY Coastal Ocean Model Version 1.0, *NRL Rep. NRL/FR/7322–00-9962*, Naval Res. Lab., Stennis Space Cent., Miss.
Melas, D., A. Lavagnini, and A. M. Sempreviva (2000), An investigation of the boundary layer dynamics of Sardinia Island under sea-breeze conditions, *J. Appl. Meteorol.*, *39*(4), 516–524.
Mellor, G. L., and T. Yamada (1982), Development of a turbulence closure model for geophysical fluid problems, *Rev. Geophys.*, *20*(4), 851–875.
Nunalee, C. G., and S. Basu (2014), On the periodicity of atmospheric von Kármán vortex streets, *Environ. Fluid Mech.*, *14*(6), 1335–1355.
Palma, J. M. L. M., F. A. Castro, L. F. Ribeiro, A. H. Rodrigues, and A. P. Pinto (2008), Linear and nonlinear models in wind resource assessment and wind turbine micro-siting in complex terrain, *J. Wind Eng. Ind. Aerodyn.*, *96*(12), 2308–2326.
Petersen, G. N., J. E. Kristjansson, and H. Ólafsson (2005), The effect of upstream wind direction on atmospheric flow in the vicinity of a large mountain, *Q. J. R. Meteorol. Soc.*, *131*(607), 1113–1128.
Petkovšek, Z., and A. Hočevar (1971), Night drainage winds, *Archiv Meteorol. Geophys. Bioklimatol., Ser. A*, *20*(4), 353–360.
Pullen, J., A. L. Gordon, J. Sprintall, C. M. Lee, M. A. Alford, J. D. Doyle, and P. W. May (2011), Atmospheric and oceanic processes in the vicinity of an island strait, *Oceanography*, *24*(1), 112–121.
Pullen, J., J. D. Doyle, T. Haack, C. Dorman, R. Signell, and C. M. Lee (2007), Bora event variability and the role of air-sea feedback, *J. Geophys. Res.*, *112*, C03S18, doi:10.1029/2006JC003726.
Pullen, J., J. D. Doyle, P. May, C. Chavanne, P. Flament, and R. A. Arnone (2008), Monsoon surges trigger oceanic eddy formation and propagation in the lee of the Philippine Islands, *Geophys. Res. Lett.*, *35*, L07604, doi:10.1029/2007GL033109.
Pullen, J., A. L. Gordon, M. Flatau, J. D. Doyle, C. Villanoy, and O. Cabrera (2015), Multiscale influences on extreme winter rainfall in the Philippines, *J. Geophys. Res. Atmos.*, *120*, 3292–3309, doi:10.1002/2014JD022645.
Reinecke, P. A., and D. R. Durran (2009), Initial-condition sensitivities and the predictability of downslope winds, *J. Atmos. Sci.*, *66*(11), 3401–3418.
Rutledge, S. A., and P. V. Hobbs (1983), The mesoscale and microscale structure of organization of clouds and precipitation in midlatitude cyclones. VIII: A model for the "seeder-feeder" process in warm-frontal rainbands, *J. Atmos. Sci.*, *40*, 1185–1206.
Sangrà, P., M. Auladell, A. Marrero-Díaz, J. L. Pelegrí, E. Fraile-Nuez, A. Rodríguez-Santana, J. M. Martín, E. Mason, and A. Hernández-Guerra (2007), On the nature of oceanic eddies shed by the Island of Gran Canaria, *Deep Sea Res., Part I*, *54*(5), 687–709.
Schär, C., and R. B. Smith (1993a), Shallow-water flow past isolated topography. Part I: Vorticity production and wake formation, *J. Atmos. Sci.*, *50*(10), 1373–1400.

Schär, C., and R. B. Smith (1993b), Shallow-water flow past isolated topography. Part II: Transition to vortex shedding, *J. Atmos. Sci.*, *50*(10), 1401–1412.

Small, R. J., S. P. Xie, L. O'Neill, H. Seo, Q. Song, P. Cornillon, M. Spall, and S. Minobe (2008), Air–sea interaction over ocean fronts and eddies, *Dyn. Atmos. Oceans*, *45*(3), 274–319.

Smith, R. B., and V. Grubišic (1993), Aerial observations of Hawaii's wake, *J. Atmos. Sci.*, *50*(22), 3728–3750.

Smith, R. B., A. C. Gleason, P. A. Gluhosky, and V. Grubišic (1997), The wake of St. Vincent, *J. Atmos. Sci.*, *54*(5), 606–623.

Teixeira, J. C., A. C. Carvalho, M. J. Carvalho, T. Luna, and A. Rocha (2014), Sensitivity of the WRF model to the lower boundary in an extreme precipitation event–Madeira island case study, *Nat. Hazards Earth Syst. Sci.*, *14*(8), 2009–2025.

Xie, S. P., W. T. Liu, Q. Liu, and M. Nonaka (2001), Far-reaching effects of the Hawaiian Islands on the Pacific Ocean-atmosphere system, *Science*, *292*(5524), 2057–2060.